Review Vol. 30, No. 6 / 14 Mar 2022 / Optics Express 8615
Optics EXPRESS

Recent developments in lanthanide-doped mid-infrared fluoride fiber lasers [Invited]

FRÉDÉRIC JOBIN,[1,3] PASCAL PARADIS,[1,3,*] YIĞIT OZAN AYDIN,[1] TOMMY BOILARD,[1] VINCENT FORTIN,[1] JEAN-CHRISTOPHE GAUTHIER,[1] MAXIME LEMIEUX-TANGUAY,[1] SÉBASTIEN MAGNAN-SAUCIER,[1,2] LOUIS-CHARLES MICHAUD,[1] SARA MONDOR,[1] LOUIS-PHILIPPE PLEAU,[1] LAURIS TALBOT,[1] MARTIN BERNIER,[1] AND RÉAL VALLÉE[1]

[1]*Centre d'Optique Photonique et Laser (COPL), Université Laval, Québec, Québec G1V 0A6, Canada*
[2]*Solutions Novika, La Pocatière, Québec G0R 1Z0, Canada*
[3]*These authors contributed equally to this work*
[*]*frederic.jobin.3@ulaval.ca*

Abstract: Mid-infrared fiber sources, emitting between 2.5 μm and 5.0 μm, are interesting for their great potential in several application fields such as material processing, biomedicine, remote sensing and infrared countermeasures due to their high-power, their diffraction-limited beam quality as well as their robust monolithic architecture. In this review, we will focus on the recent progress in continuous wave and pulsed mid-infrared fiber lasers and the components that bring these laser sources closer to a field deployment as well as in industrial systems. Accordingly, we will briefly illustrate the potential of such mid-infrared fiber lasers through a few selected applications.

1. Introduction

A great deal of work has been devoted lately to the development of coherent sources operating in the so-called mid-infrared (mid-IR) region of the electromagnetic spectrum. Now, although several definitions have been suggested for the mid-IR [1], namely the 3 μm-50 μm ISO norm [2], we will restrict the present review to the narrower spectral region starting around 2.5 μm, which corresponds to the generally accepted transmission limit of silica fibers [3] and ending around 5 μm, roughly corresponding to the long wavelength transmission edge of fluoride fibers [4]. The main motivation for developing rugged and powerful fluoride fiber-based sources naturally comes from the large number of applications enabled by light sources in the so-called 3 μm-5 μm spectral region.

Sources emitting around 2.8 μm to 2.9 μm have been particularly studied for their potential in biomedical applications in areas such as ophthalmology [5], dermatology [6], dentistry [7], biopsy [8] and angioplasty [9]. Such applications are enabled by the strong absorption of liquid water, a major component of any biological tissue, which peaks at 2.94 μm [10]. Studies of soft biological tissues have shown laser processing without the presence of charring [11]. Depending on the target tissue type and desired application, several mechanisms such as photo-chemical, thermal, photo-ablation or plasma-induced ablation will be optimal, requiring lasers operating in a variety of regimes, continuous or pulsed [12].

Other than the water vapor absorption, the mid-IR region of the electromagnetic spectra is also home to the so-called molecular fingerprint region, consisting of absorption bands of a number of basic molecular species of interest. Among these are several hydrocarbons such as methane (CH_4) around 3.2 μm-3.4 μm, ammonia (NH_3) around 3.1 μm, carbon dioxide (CO_2) around 4.3 μm and carbon monoxide (CO) around 4.6 μm [13,14]. These absorption lines also tend to be

#450929 https://doi.org/10.1364/OE.450929
Journal © 2022 Received 16 Dec 2021; revised 18 Feb 2022; accepted 18 Feb 2022; published 1 Mar 2022

Optics EXPRESS

much more intense than their near-IR counterparts by up to two orders of magnitude, originating from fundamental ro-vibrational resonances [15]. Laser sources having emission overlapping with these absorption bands or having a tunable emission could be used for remote sensing of such compounds [14,16].

Fiber lasers operating in the 3.3 μm to 3.5 μm spectral range can also be used for polymer processing. As a matter of fact, most polymers exhibit strong C-H stretch resonances in this wavelength band, which are often more intense than those observed around 10 μm, where current CO_2 laser processing systems operate. The effect of laser wavelength on ablation performances has been studied as early as 1982 [17] although efficient and powerful mid-IR sources lacked at the time. Recent studies have also shown that a laser resonant with a polymer absorption peak at 3.44 μm possesses a significantly lower ablation threshold and an enhanced material processing efficiency [18].

While the applications introduced so far took advantage of absorption bands, some benefit of the gaps left between them, especially that of water vapor. Other than the transparency window located in the visible spectrum, Earth's atmosphere exhibits two other ones located respectively between 3 μm to 5 μm and 8 μm to 12 μm. These allow for long-distance propagation of light and therefore enable applications in the field of infrared countermeasures [19] and free-space optical communications (FSOC) [20]. Defense and security applications are particularly interesting due to the overlap of the blackbody radiation emitted by aircraft turbines with these atmospheric transmission windows [19], therefore lasers emitting in this spectral region are of great interest for infrared countermeasures [21]. In the field of FSOC, the 3 μm to 5 μm band exhibits significantly less atmospheric turbulence and is therefore particularly interesting compared to the other transmission windows [22].

Although several laser sources, including quantum cascade lasers (QCLs) [23,24], optical parametric oscillators (OPOs) [25,26] and solid-state lasers based on crystalline media such as the Er^{3+}:YAG [27] or Cr- and Fe-doped chalcogenides [28], have been studied to develop light sources with adequate performances for the previously discussed applications, fiber-based sources offer significant advantages. First of all, as it is shown in Fig. 1, lanthanide ion emission cross-sections span the 2.6 μm to 4 μm range almost entirely, allowing for the generation of intense laser light at wavelengths appropriate for a number of applications. Emission beyond 4 μm has been observed in the form of fluorescence [29], but a true laser system remains to be demonstrated.

The potential of monolithic fiber lasers, which allows for extremely robust systems, is of great interest for field applications. Accordingly, although fluoride fiber components are still lagging their silica counterparts, significant progress has been made in recent years. Fiber Bragg gratings (FBGs) were among the first components developed in fluoride fibers [37,38], increasing the robustness of fiber lasers, preventing intracavity atmospheric beam propagation and reducing the onset of thermal or OH diffusion induced photo-degradation of fiber tips [39,40]. More recently, fiber combiners [41,42] and fiber-based saturable absorbers [43] were developed, leading the way to robust monolithic fluoride fiber laser systems. Strategies to mitigate some specific challenges related to the use of fluoride fibers have also been studied [44]. Altogether, these recent advances allow fluoride fiber laser systems to offer compact footprint, robust and rugged design, suitable for field applications in a variety of environments with an excellent power scalability. Finally, mid-IR fiber-based sources offer excellent beam quality, approaching $M^2 \approx 1$ when operated in a single transverse-mode regime [45].

The prior development of high quality fluoride glasses was a crucial step in the development of fiber lasers covering the 3 μm-5 μm spectral region [46]. The erbium-doped fluoride fiber laser relying on the $^4I_{11/2} \rightarrow {}^4I_{13/2}$ transition at 2.8 μm was actually the first to be demonstrated in 1988 [47], followed by a holmium laser using the $^5I_6 \rightarrow {}^5I_7$ transition at 2.9 μm in 1990 [48], the $^4F_{9/2} \rightarrow {}^4I_{11/2}$ transition at 3.5 μm of erbium in 1991 with a cryogenic cooled laser [49] and with

Optics EXPRESS

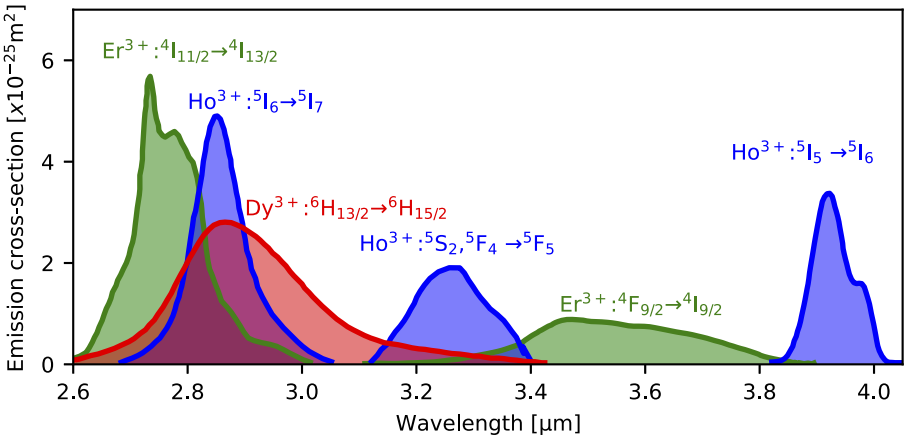

Fig. 1. Emission cross-sections of the main trivalent rare-earth ions used for mid-infrared emission. Data from: [30–36]. Holmium cross-section taken from [32], which was calculated from [33]. Measurements in fluorozirconate based glass except for the Ho^{3+}: $^5I_5$→ $^5I_6$ transition which is in fluoroindate glass.

a room temperature laser in 1992 [50], the $^5I_5$→$^5I_6$ transition at 3.9 μm of holmium in 1997 [51] and the $^6H_{13/2}$→$^6H_{15/2}$ transition at 3 μm of dysprosium in 2003 [52]. Since then, new pumping schemes, the development of fiber components and the increase in technological maturity of infrared suitable glasses have allowed mid-IR lasers to reach application ready performances. Nowadays, watt-level fluoride fiber lasers are available at several mid-IR wavelengths [53–56].

In this review, we will discuss recent progress and notable demonstrations of mid-IR fluoride fiber lasers operating in the continuous wave (CW) and pulsed regimes. We will highlight new progress related to the laser transitions spanning the 2.8 μm to 4 μm range illustrated in Fig. 1, with some emphasis on our research group's contributions. A particular consideration will be given to the components and designs which made these systems possible. Some applications enabled by these laser sources will also be discussed, notably in the fields of remote methane sensing and polymer processing.

2. Continuous wave emission in the mid-infrared

High-power fiber lasers are arguably the best option for a number of applications in industrial manufacturing such as laser welding, drilling and cleaning and the biomedical area such as tissue vaporization and ablation [57]. Among these, there has been a growing interest lately for CW mid-IR fiber lasers, which can be quite simple when no wavelength tunability is necessary so that they can adopt a monolithic design which makes them both robust and powerful. Significant breakthroughs have been made in the development of fluoride-based CW mid-IR fiber lasers through the development of suitable fiber components [41–43], novel laser schemes [58,59] and cavity design engineering [45,53], which have allowed to significantly increase the performances and robustness of CW fiber lasers. An overview of the most notable achievements reported to date as a function of wavelength is presented in Fig. 2. One clearly notes a significant decreasing trend of the power from 2.8 μm to 3.9 μm, irrelevant to the trivalent ion considered.

2.1. Erbium emission near 2.8 μm

Erbium-doped fluoride fiber lasers operating around 2.8 μm have been the most extensively studied over the last three decades [69]. Different designs have been suggested so far including wavelength-tunable lasers, pulsed lasers operating in a variety of regimes and high-power lasers.

Optics EXPRESS

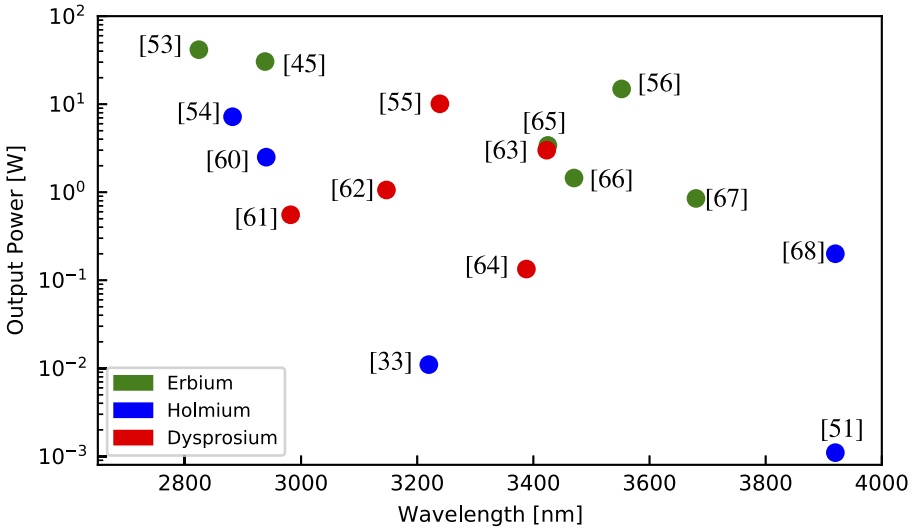

Fig. 2. Selection of reported continuous-wave notable fluoride fiber laser output power as a function of emission wavelength [33,45,51,53–56,60–68].

The simplest laser cavity design for this wavelength is made of an Er^{3+}-doped fluoride fiber bounded by two FBGs as shown in Fig. 3. Interestingly, from the manufacturing viewpoint, FBGs can now be directly written through the protective coating and into the core of a doped fluoride fiber [70–72].

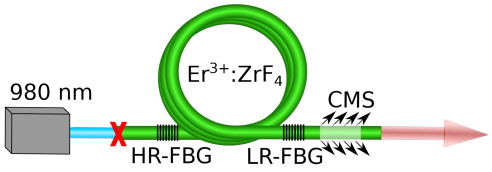

Fig. 3. Typical monolithic Er^{3+}-doped fluoride fiber laser for 2.8 μm emission. HR-FBG, highly reflective fiber Bragg grating; LR-FBG, low reflectivity fiber Bragg grating; CMS, cladding mode stripper.

Since 3 μm fiber lasers are most conveniently pumped by commercially available high-power diodes near 1 μm, the resulting Stokes efficiency of roughly 33% is a serious bottleneck to their power scaling. Scenarios for exceeding Stokes efficiency were therefore investigated in recent years, namely by using cascade lasing of the 2.8 μm and the 1.6 μm optical transitions in an erbium-doped laser cavity which resulted in a lasing efficiency of nearly 50% at 2.8 μm for a diode pumping at 976 nm [59]. Unfortunately, this promising approach was plagued with instability issues at high pumping level, preventing actual improvements in terms of high output power. The highest output power reported to date from a CW laser system around 2.8 μm is of 42 W, based on a dual-end pumped geometry [53]. Such pumping revealed crucial in distributing more evenly the significant heat load along the heavily erbium-doped fiber. A spliceless cavity design was also preferred in order to prevent unnecessary losses of the 2.8 μm radiation, which is strongly absorbed by the fiber polymer coating. For those reasons, the long-time expected demonstration of a 100 W class fluoride fiber laser has yet to come and will most likely have to rely on a new fiber design.

Optics EXPRESS

Another challenge related to the power scaling of 2.8 μm class fiber lasers is the photo-degradation problem resulting from OH diffusion [39]. This seriously hinders the long-term operation of mid-IR fluoride glass fiber lasers near 3 μm due to catastrophic failure of their fiber tips. The long-term endurance of various endcaps made of fluoride and oxide materials, namely of ZrF_4, AlF_3, GeO_2, SiO_2 and Al_2O_3 fibers have thus been investigated [44]. The degradation of these endcaps was monitored over a 100 h period at 20 W continuous-wave laser emission at 2.8 μm. It was found that a 25 nm thick diffusion barrier film made of silicon nitride (Si_3N_4) sputtered on the output face of the endcaps completely suppresses the OH diffusion into the fiber tip, thus improving drastically the resilience of high-power mid-IR fiber laser systems over long-term operation. Al_2O_3, ZrF_4 and AlF_3 endcaps with the Si_3N_4 barrier film showed no sign of degradation after being used over 100 h at 7 W as presented in Fig. 4, which is a considerable achievement since the fluoride based endcaps without this barrier film failed after less than 10 h of operation at 20 W. These results are extremely promising for the future of 2.8 μm fiber lasers, demonstrating that the crippling OH photodegradation issue can be overcome, allowing long-term operation at high powers, something essential for many applications.

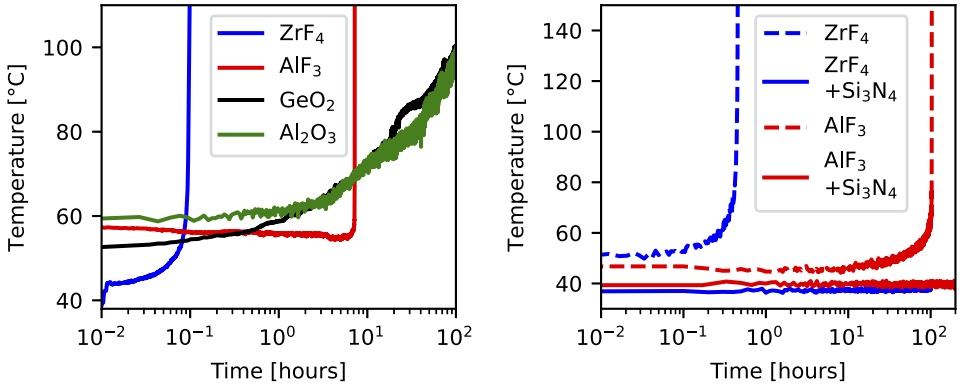

Fig. 4. (left) Evolution of the measured temperature over time for different endcaps' output face at a constant output power of 20 W and (right) the evolution of these endcaps coated with silicon nitride (Si_3N_4) at a constant output power of 7 W. Data from [44].

2.2. *Dysprosium emission from 2.9 μm to 3.4 μm*

Although mid-infrared emission from dysprosium-doped fibers was demonstrated in the early 2000s [52], most of the progress related to this ion was achieved in the past five years as can be seen in Table 1. These advances were driven by the development of a class of high-power fiber lasers operating around 2.8 μm based on the erbium ion as discussed previously. Such systems enable highly efficient in-band pumping of the dysprosium ion, allowing Stokes efficiencies reaching 91% [73]. Although several wavelengths have been studied to pump the dysprosium ion, the 2.8 μm band has given the most promising results. The 1.1 μm was the first pumping band to be studied, due to the extensive availability of ytterbium-doped fiber lasers. More recently, much interest has been given to the development of near-infrared diode-pumping, through co-doping with a sensitizing ion such as erbium or thulium. While these studies are interesting, performances achieved with such schemes have been limited up to now, with efficiencies under 6% and 260 mW for Er^{3+}/Dy^{3+} fibers [74] and of 0.3% and 12 mW for Tm^{3+}/Dy^{3+} fibers [73]. The 2.8 μm band thus remains the best candidate for high-power emission from the dysprosium ion. As a matter of fact, both the highest efficiency of 91% [73] and maximum power of 10.1 W [55] were achieved with this pumping scheme.

Optics EXPRESS

Table 1. Recent and most notable CW rare-earth doped fiber laser demonstrations in the mid-infrared

λ_p [μm]	Pump	λ_s [μm]	Host	P_{out} [W]	η [%]	Year	Ref.
0.976	Diode (clad)	2.938	Er^{3+}:ZrF_4	30	16	2015	[45]
0.976	Diode (clad)	2.825	Er^{3+}:ZrF_4	13	50	2017	[59]
0.976	Diode (clad)	2.824	Er^{3+}:ZrF_4	41.6	22.9	2018	[53]
0.976	Diode (clad)	2.8	Er^{3+}:ZrF_4	33	14	2019	[82]
0.8	Ti^{3+}:Al_2O_3 (core)	3.02	Dy^{3+}:ZrF_4	0.105	18.5	2020	[83]
0.8	Diode (clad)	3.23	Dy^{3+}/Tm^{3+}:ZrF_4	0.012	0.3	2019	[73]
0.9	Ti^{3+}:Al_2O_3 (core)	3.02	Dy^{3+}:ZrF_4	0.150	23.7	2020	[83]
0.976	Diode (clad)	3.27	Dy^{3+}/Er^{3+}:ZrF_4	0.26	5.73	2021	[74]
1.1	Yb^{3+}:SiO_2	2.98	Dy^{3+}:ZrF_4	0.554	18	2018	[61]
1.7	Raman FL	2.81-3.38	Dy^{3+}:ZrF_4	0.170	21	2018	[76]
2.8	Er^{3+}:ZrF_4	3.15	Dy^{3+}:ZrF_4	1.06	73	2018	[62]
2.8	Er^{3+}:ZrF_4	3.24	Dy^{3+}:ZrF_4	10.1	58	2019	[55]
2.8	Er^{3+}:ZrF_4	3.388	Dy^{3+}:ZrF_4	0.134	38	2021	[64]
2.8	Er^{3+}:ZrF_4	3.423	Dy^{3+}:ZrF_4	3	33	2021	[63]
0.98 + 1.9	Diode + Tm^{3+}:SiO_2	3.5	Er^{3+}:ZrF_4	0.26	25.4	2014	[77]
0.98 + 1.9	Diode + Tm^{3+}:SiO_2	3.44	Er^{3+}:ZrF_4	1.5	19	2016	[78]
0.98 + 1.9	Diode + Tm^{3+}:SiO_2	3.55	Er^{3+}:ZrF_4	5.6	26.4	2017	[40]
0.98 + 1.9	Diode + Tm^{3+}:SiO_2	3.55	Er^{3+}:ZrF_4	15	17.2	2021	[56]
0.888	Diode (clad)	3.92	Ho^{3+}:InF_3	0.200	10	2018	[68]

Another factor allowing to unleash the potential of dysprosium-doped fiber lasers was the use of FBGs. Notably, FBGs permit operation far from the emission peak at wavelengths as far as 3.42 μm in dysprosium fibers [63], and they enable high-power operation and much more robust designs by containing intracavity power within the fiber, limiting face damage due to OH degradation and thermal load [39,40]. Since dysprosium fiber lasers are almost exclusively core-pumped, the challenge resides in inscribing low-loss FBGs, which can be achieved by the phase-mask technique [38,70–72]. The use of FBGs, however, limits the tuning which can be achieved to a few nanometers [75] where free-space diffraction gratings can allow wavelength tunability spanning more than 500 nm [76].

Based on a monolithic architecture, a laser cavity was designed using a 5.5 m-long cavity bound by two FBGs inscribed directly in the active fiber (12.5/125 μm, NA=0.16, 2000 ppm), pumped by a 20 W erbium-doped fiber laser emitting at 2.8 μm as is shown in Fig. 5. The HR-FBG had a reflectivity greater than 78% and exhibited transmission losses of 8% at the pump wavelength while the LR-FBG had a reflectivity of around 20%. Their transmission spectra are shown in Fig. 6. This laser system achieved the record power of 10.1 W for a dysprosium-based laser at a wavelength of 3.24 μm as can be seen in Fig. 6 [55]. The efficiency of 58% is significantly lower than the theoretical Stokes efficiency of 87%. This difference can be explained by the low reflectivity of the HR-FBG and the somewhat too long cavity length. As a matter of fact, a numerical simulation, as shown in Fig. 6, has allowed to reproduce the experimental results achieved, considering a reflectivity of 83% for the HR-FBG and of 18% for the LR-FBG. Continuous operation over one hour at 9.3 W showed RMS fluctuations of less than 1.1%, confirming the excellent stability of this monolithic laser system.

Due to the very broad emission cross-section of dysprosium (Fig. 1) extending up to 3.4 μm, this ion has been considered as an alternative source for efficient polymer processing applications.

Optics EXPRESS

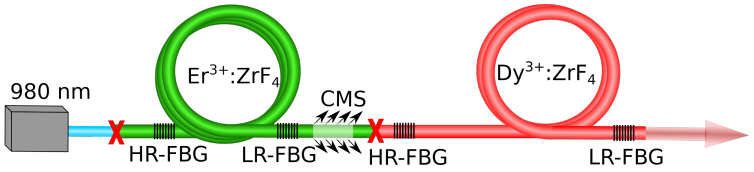

Fig. 5. Typical monolithic Dy^{3+} laser cavity experimental setup. HR-FBG, highly reflective fiber Bragg grating; LR-FBG, low reflectivity fiber Bragg grating; CMS, cladding mode stripper; x, splice.

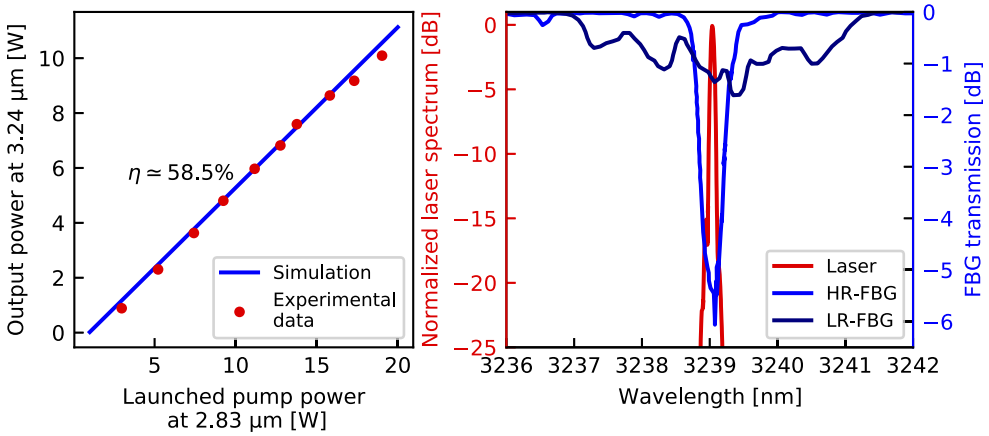

Fig. 6. (left) Laser output power at 3.24 μm as a function of the launched pump power at 2.8 μm and (right) transmission spectra of the FBGs bounding the 3.24 μm laser cavity and output spectrum of the Dy^{3+} fiber laser.

As a matter of fact, recent developments in dysprosium-doped fiber lasers have allowed achieving output powers in the range of a few watts at a wavelength of 3.42 μm, which is comparable to power levels achieved from dual-pumped erbium-doped fiber lasers [63,65] (Fig. 2). Once again a monolithic cavity design as the one shown in Fig. 5 was used. This time the cavity had a length of 5.6 m of dysprosium-doped fiber (16/250 μm, NA=0.12, 2000 ppm) bound by two FBGs with reflectivities of 95% and 39% at 3.423 μm. A power of 3 W with a slope efficiency of 33% and pump threshold power of 2.22 W were achieved as can be seen in Fig. 7 [63]. The laser output power was limited by thermal damage to the fiber caused by the scattered 3.423 μm radiation from the FBGs and the splice point which is heavily absorbed by the fiber's polymer coating.

2.3. *Erbium emission near 3.5 μm*

Emission from the 3.5 μm band of trivalent erbium-doped fibers was demonstrated as early as 1992. However the pumping wavelength of 655 nm showed severe bottlenecking of the ions on the lower energy levels, causing a poor slope efficiency of 2.8% [50]. It took over twenty years before this laser transition became the subject of further significant research enabled by the brilliant proposition of a dual-wavelength pumping scheme which allowed circumventing the bottlenecking effect and resulting in 260 mW output power with an overall optical efficiency of 16% [77]. With this technique using a 980 nm pump to create a virtual ground state and a 1.9 μm laser to pump the $^4F_{9/2}$ level, performances increased as the systems became more and more all-fiber and eventually monolithic [40,56,78] with the development of silica to fluoride single-mode splices [79]. These demonstrations used 1 mol.% Er^{3+}-doped fiber which causes a

Optics EXPRESS

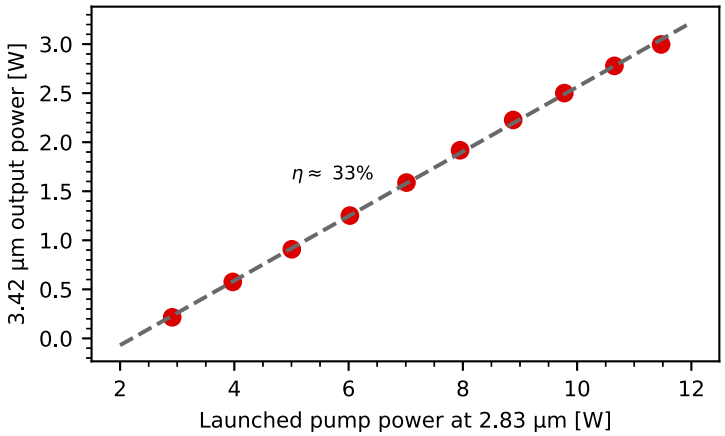

Fig. 7. Laser curve of the 3.42 µm Dy^{3+} fiber laser as a function of 2.83 µm launched power. Data from [63].

quenching of 3.5 µm laser emission if insufficient 980 nm pump is applied to the system due to the excited-state absorption at 1.9 µm [80]. Heavily doped fibers do not suffer from this phenomenon and have proven to be a candidate for 3.5 µm emission, although thermal issues may arise [65].

Recently, using a fully monolithic setup for the first time, as illustrated in Fig. 8, up to 15 W of output power at 3.55 µm was achieved with an overall optical efficiency of 17.2% and a slope efficiency of 51.3% [56]. A 2.1 m-long segment of fiber (11/240×260 µm, NA=0.125, 10 000 ppm) bounded by two FBGs with reflectivities of 92% and 26.9% was used. The fiber length was chosen in accordance to numerical simulations [56]. Since core pumping is used for the 1976 nm signal, FBGs with low losses are crucial and a careful inscription allowed to limit them to 2.9%. The overall optical efficiency is lower than previously reported [40], likely due to the important residual pump power. The laser curve, illustrated in Fig. 9, exhibits the typical quenching phenomenon described previously [80]. The high residual pump power was a result of the short fiber length and high 980 nm pumping required by numerical simulations to maximize the slope efficiency and output power. This once again shows the potential of fully monolithic systems, allowing increasing the previous output power record by a factor of nearly three.

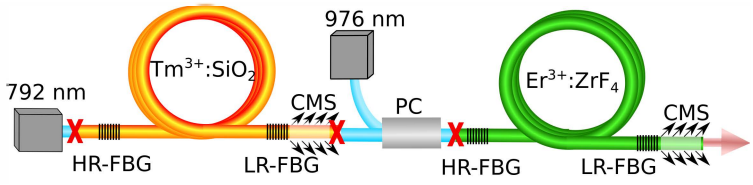

Fig. 8. Typical monolithic 3.5 µm-band Er^{3+} laser cavity experimental setup. HR-FBG, highly reflective fiber Bragg grating; LR-FBG, low reflectivity fiber Bragg grating; CMS, cladding mode stripper; PC, pump combiner; X, splice.

2.4. *Holmium emission near 3.9 µm*

The first fiber laser producing 11 mW of output power at 3.9 µm form a zirconium fluoride based fiber was reported by Schneider *et al.* in 1997 [51], but it required liquid nitrogen cooling and core pumping by Ti:Sapphire laser to reach the lasing threshold. Significant progress has since been made in the development of low phonon energy soft glass and in the spectroscopic

Optics EXPRESS

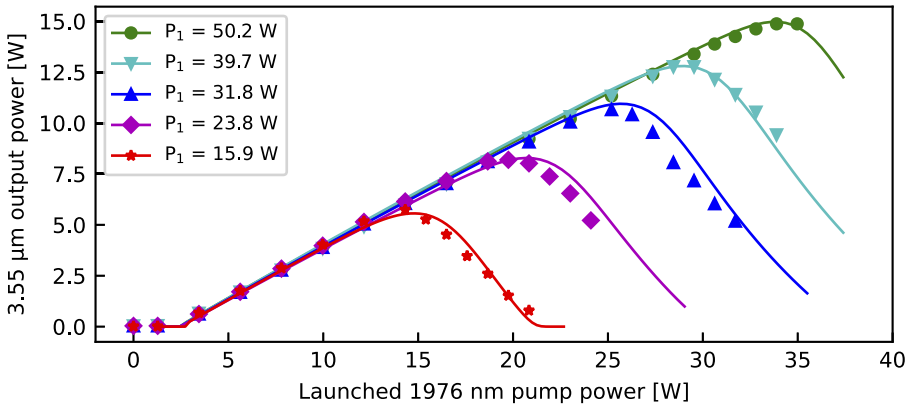

Fig. 9. Experimental (dots) and simulated (lines) 3.55 µm output power as a function of the 1976 nm launched pump power for varying levels of the 976 nm pump. Data from [56].

investigations of the holmium ion [36,81]. In 2018, Maes *et al.* demonstrated the highest output power emitted at 3.92 µm with an average output power of 200 mW at room temperature using a double-clad Ho^{3+}:InF_3 fiber and a lasing efficiency of 10% with respect to the launched pump power [68].

3. Pulsed emission in the mid-infrared

As for high-power CW mid-IR fiber lasers, pulsed mid-IR lasers are also of great interest for several fields including biomedical applications [57,84], material processing [57,85,86], remote sensing [14,15,87–89] and non-linear optics [57]. Since the optimal pulse characteristics are application specific, the development of a wide variety of laser sources producing varied repetition rates, pulse energies, pulse durations and peak powers is of great importance. Several techniques have been studied over the past decade for the generation of such mid-IR emission, namely *Q*-switching, gain-switching and mode-locking. With the growing interest for pulsed mid-IR laser sources, novel fiber and bulk components have been developed over the years although fiberized components are still lacking in commercial availability. Almost all of the reported demonstrations of pulsed mid-IR fiber lasers in the literature use an architecture combining free space optics with optical fiber components making these lasers unsuitable for field deployment because of their inherently unreliable optical alignment. In recent years, our group has focused on the development of fiberized components for the mid-IR, aiming to improve the robustness of the design of pulsed fiber sources. A notable example is the fuseless side-pump combiner to launch pump power into the cladding of a double-clad fluoride fiber [42,90] that is arguably simpler to manufacture than an angle-fused side-pump combiner [41,91,92]. This new and highly efficient pump-combiner can also sustain the thermal load inherent to high-power mid-IR fiber lasers and amplifiers.

3.1. *"Long" pulse generation in the mid-infrared*

We define here "long" pulses as those for which the duration is in the nanosecond to microsecond range. Such pulses are of great interest for a number applications in the fields of remote sensing [14,15,93,94] and material processing [86,95,96]. Two main techniques allow the generation of such pulses, *Q*-switching and gain-switching, both relying on the ratio of gain to losses in a laser cavity. Gain-switching can make use of the same monolithic architecture as CW devices, since pulses are generated by electronically modulating a laser diode [97]. Another advantage of this approach is the potential for high-power operation, since such lasers are not limited

Optics EXPRESS

by the damage threshold of 2D material saturable absorbers. *Q*-switching, however, generally requires an intracavity loss mechanism, such as an acousto-optic modulator (AOM) in the case of active switching or a passive saturable absorber in the case of passive switching as shown in Table 2. Until very recently, there were no real all-fiber loss mechanisms optimized for the mid-IR which makes these *Q*-switched fiber lasers unreliable in the harsh environments of most field applications.

Table 2. Recent and notable pulsed rare-earth-doped mid-infrared fiber system demonstrations (QS: *Q*-switching, GS: Gain-switching, LP: Linearly Polarized, AOM: Acousto-optic modulator, BP: Black phosphorus, MOPA: Master Oscillator Power Amplifier)

Mechanism	Ion	λ_s [μm]	P_{pk} [W]	E_p [μJ]	Duration [ns]	Rep. rate[kHz]	Ref.
QS (AOM)	Er^{3+}	2.8	900	100	90	120	[103]
QS (AOM)	Er^{3+}	2.79	10.6×10^3	560	53	1	[104]
QS (AOM)	Er^{3+}	2.78	12.7×10^3	330	26	0.1	[105]
QS (Dy^{3+}:SiO_2)	Er^{3+}	2.791	–	3.3	250	250	[43]
QS (BP)	Er^{3+}	2.7715	—	0.82	3320	22.2	[106]
QS (Sb-SAM)	Er^{3+}	2.7997	—	1.03	1700	58.8	[107]
QS (MoS_2)	Er^{3+}	2.754	—	2	806	70	[108]
QS (SESAM)	Er^{3+}	2.7949	21.9	6.9	315	146.3	[109]
QS (Fe^{2+}ZnSe)	Er^{3+}	2.78	5.34	2	370	161	[110]
QS (EOM)	Er^{3+}	2.7	15.7×10^3	205.7	13.1	0.1-50	[111]
QS (SESAM, LP)	Er^{3+}	2.7-2.83	—	4.77	1170	97.61	[112]
QS (AOM)	Dy^{3+}	2.97 - 3.23	—	12	270	0.1–20	[113]
QS (BP)	Dy^{3+}	3.04	—	1	740	86	[113]
QS (PbS)	Dy^{3+}	2.71 - 3.08	—	1.88	795	166.8	[114]
QS (AOM)	Er^{3+}	3.47	—	7.8	500-1100	5-100	[115]
QS (self)	Er^{3+}	3.45	—	<1	—	19-29	[116]
QS (SESAM)	Er^{3+}	3.46	—	1.4	2470	26.83-58.71	[117]
QS (Fe^{2+}:ZnSe)	Er^{3+}	3.4-3.7	—	7.54	1180	71.43	[118]
QS (BP)	Er^{3+}	3.46	—	1.8	2050	55-66	[119]
GS	Er^{3+}	2.8	68	20	300	100	[120]
GS	Er^{3+}	2.826	345	80	170	140	[97]
GS (LP)	Er^{3+}	2.7-2.82	—	4	1040	20	[112]
GS	Dy^{3+}	2.8 - 3.1	—	4.36	530	40/80	[121]
GS	Dy^{3+}	2.94	4	0.72	183	25-100	[122]
GS	Dy^{3+}	3.24	18	19.3	300-800	20-120	[123]
GS	Er^{3+}	3.55	200	6.5	30-50	12-20	[124]
GS	Er^{3+}	3.46	6	10.1	1600-3200	100	[125]
GS	Er^{3+}	3.4-3.7	—	5.29	1020	50	[126]
MOPA	Er^{3+}	2.79	10^6	1000	0.986	5	[127]
MOPA	Er^{3+}	2.72	60.3×10^3	670	11.5	0.01	[128]

The development of all-fiber saturable absorbers is likely to enable a new generation of robust mid-IR *Q*-switched lasers. Accordingly, it was shown recently that a Dy^{3+}-doped silica fiber can be used as saturable absorbers in a *Q*-switched mid-IR truly all-fiber laser [43], in the same way as it was first demonstrated for the near-infrared fiber lasers [98–102]. This kind of saturable absorber based on a rare-earth-doped silica fiber has an increased damage threshold due to the

Optics EXPRESS

volumetric absorption compared to the surface absorption of 2D materials. Moreover, it can be fusion spliced to the rest of the laser system, further improving the robustness and reliability of the laser design. A schematic of the experimental setup is presented in Fig. 10. As can be observed in Fig. 11, the performances of this mid-IR Q-switched fiber laser emitting at a wavelength around 2.8 µm with pulses as short as 240 ns at a repetition rate of 120 kHz are comparable to other passively Q-switched fiber lasers as observed in Table 2 presenting a literature overview of those sources. The average power was not very high at about 400 mW because the demonstration was focused mostly on the proof of concept and assessing the limitations of this design. From the general behavior of this prototype, it appears that the Q-switched pulse train is stable, although it is not yet based on an all-fiber design. It also appears that the average power could be significantly increased since there is no sign of saturation in the laser output power, thus keeping the laser cavity stable and robust. Moreover, this preliminary test showed that it is now possible to design a mid-IR Q-switched truly all-fiber laser cavity using previously developed fiber components for the mid-IR. The latest developments from this project i.e., the experimental demonstration of a Q-switched truly all-fiber laser design has been recently submitted for publication.

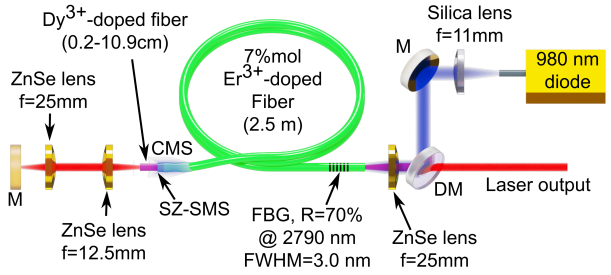

Fig. 10. Experimental setup of mid-IR Q-switched fiber laser using a Dy^{3+}-doped silica fiber as a saturable absorber. (CMS: cladding mode stripper; DM: dichroic mirror; FBG: fiber Bragg grating; M: gold mirror; SZ-SMS: silica-fluoride glass single-mode splice)

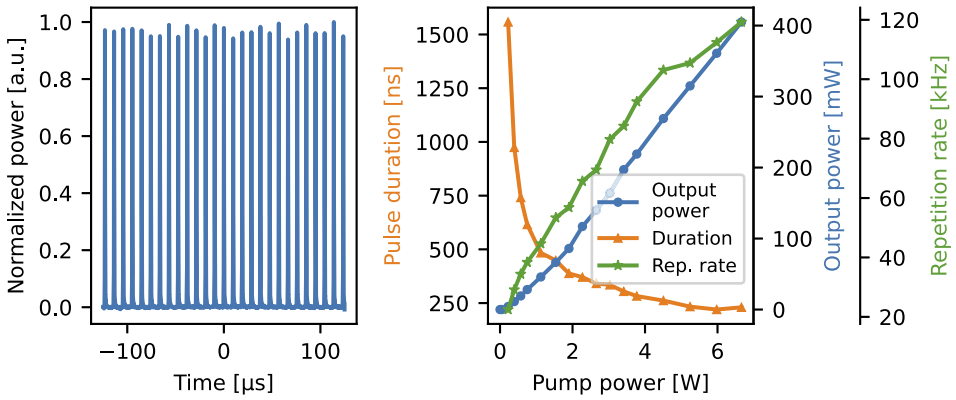

Fig. 11. (left) Pulse train example of the mid-IR Q-switched fiber laser using a Dy^{3+}-doped silica fiber as a saturable absorber and (right) its output power, pulse duration and repetition rate curves.

The development of pulsed fluoride fiber lasers operating beyond 3 µm is fairly recent and followed that of CW lasers at those longer wavelengths as well as that of pulsed lasers around 2.8 µm. The first band to be investigated was the erbium's 3.5 µm one for which gain-switching [124] and active Q-switching [115] were demonstrated quasi-simultaneously,

Optics EXPRESS

producing respectively 6.5 μJ and 7.8 μJ at 15 kHz. In the following years, several saturable absorbers were tested, generating pulses of less than 10 μJ (Table 2). Gain-switching has allowed achieving watt-level average power at 3.46 μm with pulse energies of up to 10.1 μJ [125]. Although emission quenching was observed in the first demonstration of 3.5 μm gain-switching [124], this time it was not observed, most likely due to the longer pulse duration and lower peak power [125]. In both *Q*-switching and gain-switching, tunable emission ranging from 3.4 μm to 3.7 μm was also achieved [118,126] using a plane ruled grating.

Dysprosium was the next candidate to be studied for pulsed emission beyond 3 μm. Although its emission peak is at 2.9 μm, this ion is of particular interest to bridge the "erbium gap" between 3 μm and 3.4 μm due to its very broad emission cross-section (Fig. 1). As stated previously, CW emission has proven that high-power emission from dysprosium is possible far from the emission cross-section's peak [55,63]. Nonetheless, most pulsed dysprosium-doped lasers operate at or below 3.1 μm (Table 2). The longest emission wavelength for a long-pulse dysprosium laser was of 3.23 μm, from an actively *Q*-switched tunable laser that produced up to 12 μJ of energy at 3.1 μm [113]. Gain-switched dysprosium based systems were also demonstrated, using a 1.1 μm pulsed laser as a pump [121,122]. Tunable operation was thus achieved from 2.8 μm to 3.1 μm with a maximum pulse energy of 4.36 μJ [121].

An in-band pumped monolithic dysprosium fiber laser was reported recently, featuring the record average output power and pulse energy for a fiber laser operating beyond 3 μm. The system presented in Fig. 12, produced up to 1.4 W of average power and 19 μJ pulses at 3.24 μm [123]. This system consisted of a 1.75 m-long segment of dysprosium-doped fluoride fiber(16/250 μm, NA=0.12, 2000 ppm) bounded by two FBGs inscribed directly in the active fiber. The FBGs' reflectivities were greater than 99.5% for the HR and approximately 65% for the LR. The laser was pumped by a 2.8 μm pulsed source consisting of an oscillator similar to the one described by Paradis *et al.* [97] and of a fiber amplifier. Pulse energy as a function of the repetition rate and the pump pulse energy is shown in Fig. 13 for stable pulsed operation. It was achieved between 20 kHz and 120 kHz and the operation limits were due to the 2.8 μm pumping system. The modest 22% efficiency is likely due to a combination of splice and HR-FBG losses combined to a strongly reflective output coupler. Its value was chosen with the help of numerical simulations to maximize the operation range in terms of repetition rates. Although some free space components were required for this system, the 3.24 μm cavity itself was monolithic and one can hope that a fully optimized pumping source will allow an entirely monolithic system in a near future. The design and optimization of pumping sources and the study of various pumping schemes will be critical for the future progress of pulsed dysprosium-doped fiber lasers.

An alternative approach was considered lately for generating high energy pulses in the mid-IR based on MOPA systems seeded either by OPG or OPA modules. A system was first reported to generate 24-ps-long pulses with an energy of 84 μJ [129]. Aydin *et al.* demonstrated a MOPA system able to produce nanosecond-level pulses around 2.8 μm with an average power of 2.45 W and a pulse energy of 122 μJ at 20 kHz [53], but free space propagation and geometry mismatch between the different fibers of the amplifier led to fiber tip failure and power instabilities. Then, Du *et al.* demonstrated an amplifier system seeded by an OPA that generated 11.5 ps-long pulses with a pulse energy of 670 μJ at 2.72 μm, but the average power of the signal was limited to 7 mW. Very recently, Aydin *et al.* reported on a dual-stage amplifier system outputting 1 ns pulses at 2.8 μm with a pulse energy of 1 mJ and an average power of 5 W at 5 kHz [127]. The first stage is made of an erbium-doped fluoride fiber with a core diameter of 85 μm while the second stage is also composed of an erbium-doped fluoride fiber, but with a core diameter of 115 μm. This system made use of the fuseless side-pump combiner previously introduced [42] to pump the fibers bidirectionally and thus more efficiently. This scheme, involving cladding mode strippers at all ends, also contributed to preventing pump coupling and thus heat load issues at the fiber tips, as shown in Fig. 14. Moreover, these side-pump combiners made this laser system

Optics EXPRESS

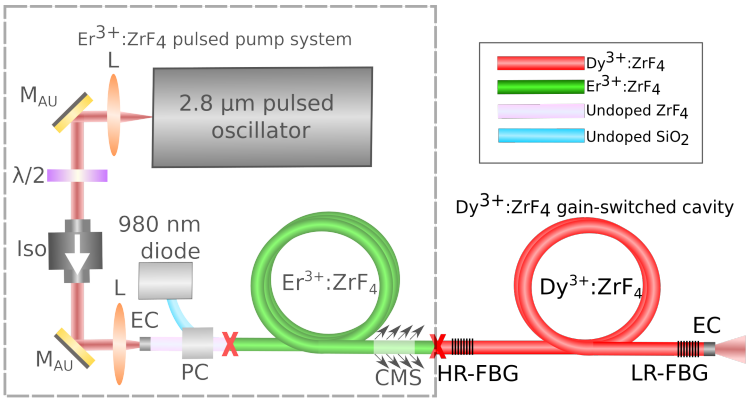

Fig. 12. Experimental setup of the gain-switched Dy^{3+}-doped fiber laser at 3.24 µm. L, ZnSe lens; M_{AU}, gold mirror; $\lambda/2$, half-wave plate; Iso, optical isolator; EC, endcap; PC, pump combiner; CMS, cladding mode stripper; HR-FBG, highly reflective FBG, LR-FBG, low-reflectivity FBG; X, splice. Reprinted with permission from [123] © The Optical Society.

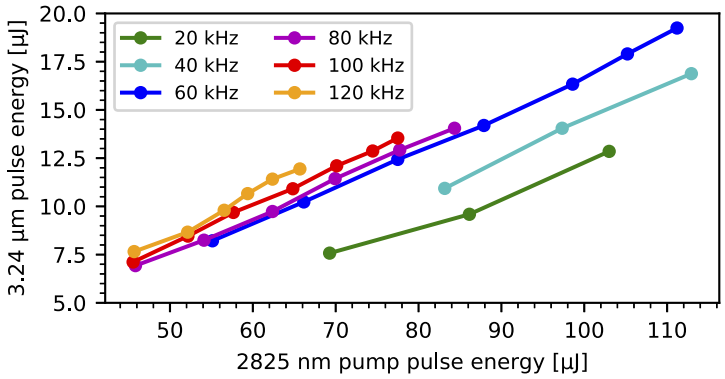

Fig. 13. 3.24 µm pulse energy as a function of the 2.8 µm pump pulse energy for repetition rates ranging from 20 kHz to 120 kHz. Data from [123].

more resilient to high power and eased the alignment requirement. The average output power showed an RMS fluctuation of about 1.5% over a 2h-long stability test at 5 W. Due to their short duration and yet large pulse energy, such 3 µm-class pulses were shown to be perfectly designed for biomaterial processing, leading to essentially no collateral damage of the surrounding area of the laser focus point [130].

3.2. Ultrafast pulse generation in the mid-infrared

Just like pulses in the microsecond and nanosecond ranges, pulses in the picosecond to femtosecond range are also interesting for remote sensing and material processing but also for more exotic applications such as high-harmonic generation [131]. Because of the great potential of these laser sources, a great deal of effort is made towards shortening the pulses, increasing the peak power, extending to longer wavelengths and improving the robustness and simplicity of the laser designs, as can be seen in Table 3. The first mode-locked fiber lasers emitting femtosecond pulses in the mid-IR near 2.8 µm were developed by two different research groups at about the same time [132,133]. Using the non-linear polarization evolution (NPE) mode-locking scheme,

Optics EXPRESS

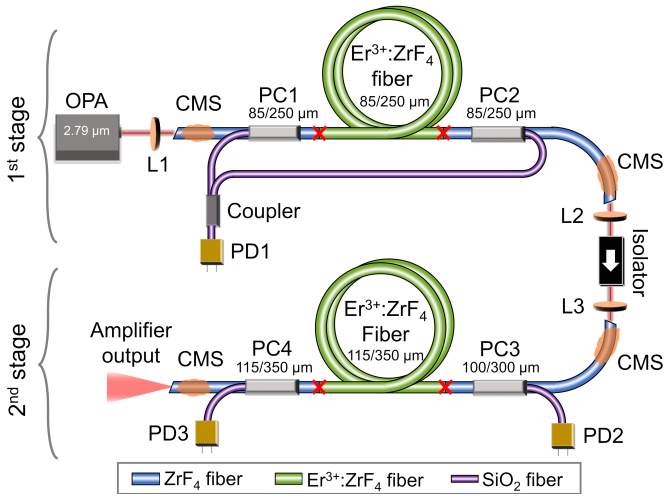

Fig. 14. Dual stage fiber amplifier outputting millijoule-level sub-nanosecond pulses with an average power of 5 W near 3 µm. Reprinted with permission [127] © The Optical Society.

these ring-cavity lasers generate soliton pulses that are very close to the Fourier transform limit. Shortly after, the peak power from these lasers were increased to a few tens of kilowatts [134,135]. It has been demonstrated that these soliton pulses can also be shifted to much longer wavelengths by soliton self-frequency shift (SSFS) when amplified and propagated through a fiber segment of appropriate length [136]. This SSFS phenomenon also has the advantage of cleaning up the main soliton from the Kelly side bands resulting in a very clean main soliton when proper caution is taken for the design of the laser amplifier system. Dispersion and chirp management in amplifiers, have recently allowed ultrafast sources to achieve sub-two-cycle pulses [137] and peak powers up to 2 MW [138].

More recently, this SSFS technique was pushed further based on the same soliton mode-locked seed but with a 20 m-long 7.5 µm diameter core InF_3 fiber spliced to the Er^{3+}-doped fluoride fiber amplifier. The smaller core of the InF_3 fiber increased the non-linear effects on the soliton by reducing the effective mode area by a factor of 4 and thus increasing the peak intensity of the pulses accordingly. The smaller core also contributed to shifting the dispersion parameter of the fiber as recently determined precisely by Boilard *et al.* [156]. Lastly, since the InF_3 fiber transparency extends to 5.2 µm, as opposed to 4.2 µm for the ZrF_4 fiber, the solitons were allowed to shift up to 4.62 µm without being affected by propagation losses (cf. Fig. 15 [155]).

In the perspective of somehow coping with the current lack of robust and ideally fiberized mid-IR components, efforts were made to simplify the design of mid-IR mode-locked fiber lasers, namely by adopting linear cavities that are taking advantage of the strength and simplicity of CW laser's architecture. Some promising results were obtained with a linear laser cavity making use of an FBG as output coupler to stabilize the laser emission wavelength in 2015 [157]. This demonstration was followed by another take on a linear architecture that could generate much shorter pulses with a duration of 25 ps [139]. A few years later, we developed a linear laser cavity bounded by an FBG and a SESAM that could generate 15 ps pulses [140] centered around 2791 nm. However, as studied by Majewski *et al.* [158], the pulse duration seemed to be limited by the spectral bandwidth limitations cause by the water vapor absorption features around 2.8 µm. The free-space propagation of the laser beam with a spectrum centered around 2.8 µm is thus one of the limiting factors to improve the performances of these lasers. Very recently, using a home-made MXene saturable absorber mirror, Bharathan *et al.* could demonstrate an almost all-fiber design as seen in Fig. 16, very similar to other "all-fiber" mode-locked lasers in the near

Optics EXPRESS

Table 3. Recent and notable ultrafast fiber laser demonstrations in the mid-infrared. NPE: Non-linear polarization evolution, BP: Black phosphorus, FSF: Frequency-shifted feedback, GNW: gold nanowires LP: linearly polarized, CEFA: Chirped engineered fiber amplifier, DMFA: Dispersion-managed fiber amplifier, SSFS: Soliton self-frequency shift.

Host	Mechanism	λ_s [μm]	Bandwidth [nm]	P_{pk} [kW]	E_p [nJ]	Duration [ps]	Rep. rate [MHz]	Ref.
Er^{3+}	SESAM	2.8	4.8	1.86	44.3	25	22.56	[139]
Er^{3+}	SESAM	2.791	0.65	—	2.7	15	55	[140]
Er^{3+}	Mxene	2.796	0.721	—	16	—	37	[141]
Er^{3+}	Fe^{2+}:ZnSe	2.8	0.6	0.049	0.93	—	50	[142]
Er^{3+}	BP	2.8	2.8	0.608	25.5	42	24	[143]
Er^{3+}	BP	2.7711	4.9	—	0.23	—	27.4	[106]
Er^{3+}	Graphene	2.8	0.21	0.017	0.7	42	25.4	[144]
Er^{3+}	SESAM	2.8 (LP)	—	—	—	44	22.03	[145]
Er^{3+}	NPE	2.875-2.81	—	10.9	2.6	0.199-0.27	52.3	[146]
Er^{3+}	NPE+CEFA	2.8	—	500	11	0.016	42.1	[137]
Er^{3+}	NPE+DMFA	2.8	200	2000	101	0.049	37.7	[138]
Ho^{3+}	SESAM	2.87	4.2	0.2	4.9	24	27.1	[147]
Ho^{3+}	SESAM	2.86	5	0.465	2.79	6	24.8	[148]
Ho^{3+}	Bi_2Te_3	2.83	10	1.43	8.6	6	10.4	[149]
Ho^{3+}/Pr^{3+}	GNW	2.865	8.1	0.311	3.7	12	26.08	[150]
Er^{3+}	NPE	2.8	—	3.5	0.8	0.207	55.2	[132]
Er^{3+}	NPE	2.793	20.1	6	3.6	0.497	56.7	[133]
Er^{3+}	NPE	2.8	—	23	7	0.27	96.6	[134]
Ho^{3+}	NPE	2.876	60	37	7.6	0.18	43.1	[135]
Dy^{3+}	FSF	2.97 - 3.3	0.33	—	2.7	33	44.5	[151]
Dy^{3+}	NPE	3.1	13.7	4.2	4.8	0.828	60	[152]
Er^{3+}	BP	3.49	4.7	—	1.38	—	28.91	[119]
Er^{3+}	FSF	3.47	0.58	—	1.38	0.053	36.23	[153]
Er^{3+}	NPE	3.54	23	5.5	3.2	0.58	68	[154]
Er^{3+}	NPE + SSFS	2.8→3.6	—	9.5→109	4.7→30	440→250	57.9	[136]
Er^{3+}	NPE + SSFS	2.8→4.62	—	9.5→?	4.7→?	440→?	57.9	[155]

infrared with a spectral bandwidth of 721 pm, corresponding to a Fourier limited pulse duration of 11.4 ps [141]. In general, though, the mode-locked pulses generated by this kind of linear cavity are longer than similar pulses generated by ring cavity using NPE and even those using material saturable absorber such as SESAM and other 2D materials as can be seen in Table 3.

The development of ultrafast laser sources beyond 3 μm has also been a topic of interest. Due to its extremely broad emission cross-section extending beyond 3 μm, the dysprosium ion is a promising candidate for such ultrafast laser emission. Frequency-shifted feedback (FSF) [159] was first used to generate picosecond pulses. Using an acousto-optic tunable filter, 33 ps pulses with energies up to 2.7 nJ were generated in a laser tunable from 2.97 μm to 3.3 μm [151]. The first sub-picosecond pulses were generated in a ring cavity using non-linear polarization evolution [152]. The experimental setup of this laser can be seen in Fig. 17. A dysprosium-doped fluoride fiber (12.5/125 μm, NA=0.16, 2000 ppm) was core-pumped by a 2.8 μm laser in a co-propagating configuration. Two fiber lengths were tested, 3 m and 4.5 m, and the output coupler reflectivities were approximately of 22.5% and 55% at 3.1 μm. Self-starting mode-locked pulses as short as

Optics EXPRESS

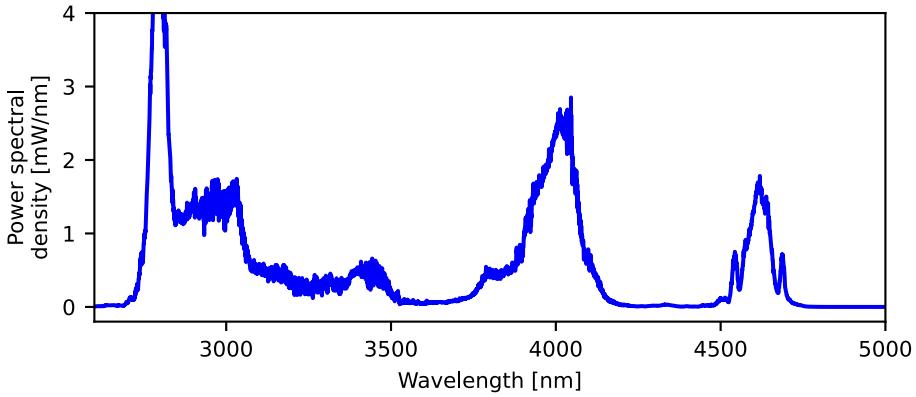

Fig. 15. Soliton self-frequency shift from 2.8 μm up to 4.6 μm [155]

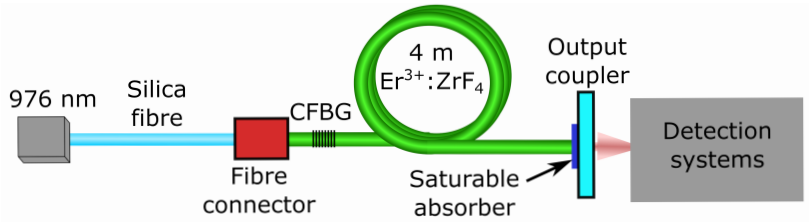

Fig. 16. Mid-IR mode-locked all-fiber laser based on a home-made MXene saturable absorber. CFBG: chirped fiber Bragg grating. Adapted with permission from [141] © The Optical Society.

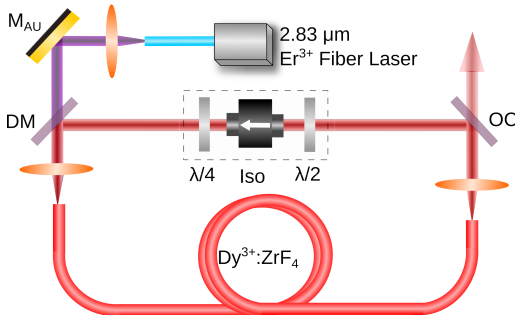

Fig. 17. Experimental setup of the ultrafast Dy^{3+} laser at 3.1 μm. M_{AU}, protected gold mirror; DM, dichroic mirror, CMS, cladding mode stripper; OC, output coupler; $\lambda/4$, quarter-wave plate; $\lambda/2$, half-wave plate; Iso, optical isolator.

828 fs were generated at 3.05 μm for the 3 m fiber and of 1.01 ps at 3.083 μm for the 4.5 μm fiber. A maximum pulse energy of 4.8 nJ corresponding to a peak power of 4.2 kW was achieved at a repetition rate of 60 kHz with the larger output coupler. The important anomalous dispersion of the fiber is a significant issue to produce shorter pulses at those longer wavelengths, which could be observed from the numerous Kelly sidebands present in the laser spectrum as can be seen in Fig. 18. The area theorem [160], gives an approximate pulse duration of 1 ps, which is in agreement with experimental results [152]. Time-bandwith products of 0.39 and 0.43 were calculated for the 3 m and 4.5 m fiber, close to the limit of 0.315 for a hyperbolic secant pulse.

Optics EXPRESS

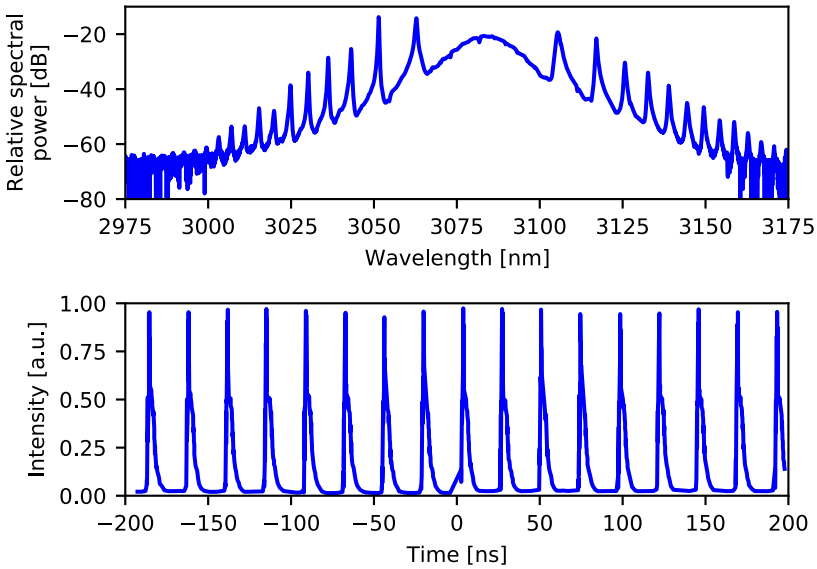

Fig. 18. (top) Optical spectrum of the mode-locking pulse train measured with the OSA at 0.2 nm resolution and (bottom) temporal trace of the mode-locked pulse train for a 4.5 m fiber. Data from [152].

Ultrafast sources in the 3.5 μm band of erbium were achieved thanks to the dual-wavelength pumping scheme. Initially, mode-locking was observed using a black phosphorous saturable absorber, although no full characterization was available since no autocorrelation trace could be measured [119]. Later on, the FSF mechanism was used to generate 53 ps pulses ranging from 3.4 μm to 3.7 μm [153]. This system operated in a single pulse regime at 36.23 MHz with pulse energies of 1.38 nJ while multi-pulse operation was observed if the pumping power was increased. Recently, using non-linear polarization evolution in a ring cavity, 580 fs pulses were generated at a repetition rate of 68 MHz, corresponding to a pulse energy of 3.2 nJ and peak power of 5.5 kW [154].

4. Selected applications of mid-infrared fiber lasers

4.1. Methane sensing

Although its average concentration in the atmosphere is more than 200 times less than that of carbon dioxide, methane has, on a weight basis, a 21 times larger global warming potential and is thus considered as an alarming greenhouse gas [161]. Up to now, multiple detecting and measuring scheme for greenhouse gases' fluxes and concentrations have been demonstrated using eddy current analysis, flux boxes and optical devices operating in the near or mid infrared [15,93,162,163]. A particularly interesting approach is using a hyperspectral camera to provide an image of methane concentration [164]. Methane, like most atmospheric greenhouse gases, presents strong absorption bands in the mid-infrared. Sources emitting such wavelengths have been used for the remote detection of methane [93,165,166] and the development of robust, powerful and compact fiber laser sources spanning such wavelength bands, notably using the dysprosium and erbium ions has created new alternatives.

Tunable laser absorption spectroscopy (TLAS) is one of the techniques allowing the detection of methane or other chemical compounds using a narrow laser band [167]. For the case of methane, its absorption band near 3.24 μm illustrated in Fig. 19, is of particular interest, being accessible through laser emission from dysprosium fiber lasers [55,75,123] and being sufficiently

Optics EXPRESS

separated from surrounding water vapor absorption lines. In a monolithic dysprosium doped fiber laser emitting at 3.24 μm similar to the one shown in Fig. 5, the FBGs can force emission between these two bands and then be tuned to scan the methane absorption band and, if desired as illustrated in Fig. 19, the water band to determine both concentrations. In this case, the FBG was tuned thermally using a commercial module from the company *Teraxion*. A similar approach has also been applied for the 3.427 μm band of methane, using a dual-wavelength pumped erbium doped fiber laser which was mechanically tuned using a piezoelectric bending beam [168]. Although the tuning range achieved with this technique is only of a few nanometers, compared to the hundreds of nanometers achievable with a free-space diffraction grating [169] or an acousto-optic tunable filter [170], this allows a fully monolithic and therefore robust and stable design, two essential features for real-world field applications.

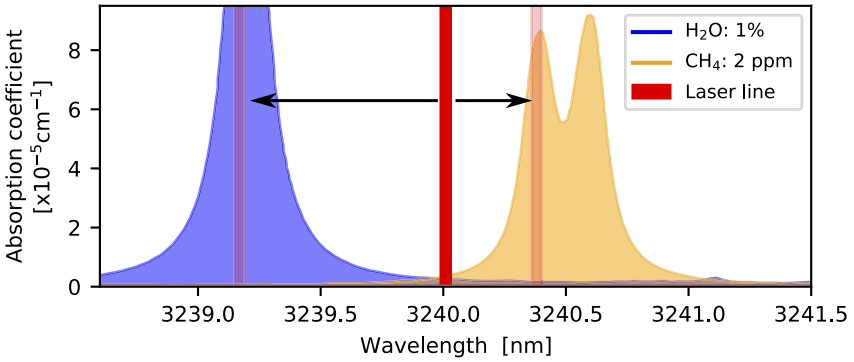

Fig. 19. Tunable laser absorption spectroscopy of methane at 3.24 μm

Detecting multiple gas at once while keeping a simple detection system is another challenge where mid-infrared light sources can prove useful, due to the strong absorption of molecules in this spectral region. By using the photoacoustic effect, which results from the time-modulated absorption of light by a target gas causing it to create sound waves, the gas concentration can be measured using a simple microphone instead of a bulky spectral measurement device (e.g., monochromator, spectrograph). This is especially appealing when working in the mid-infrared region, since sensitive detectors and optical components can be much more expensive than their near-infrared counterparts. In a proof-of-concept experiment, a broad spectrum light source (a mid-IR supercontinuum in this case [155]) was used to detect set concentrations of methane (CH_4). A schematic of the experimental setup is shown in Fig. 20. The laser beam first propagates through a hermetic cell containing a known concentration of the target gas, which mimics atmospheric propagation. As a result, the light at the wavelengths corresponding to the CH_4 absorption lines is partially absorbed proportionally to the gas concentration. A mechanical chopper then modulates the light intensity before the beam gets focused in a small 225 mm long x 2.5 mm diameter non-resonant hermetic photoacoustic cell filled with a fixed concentration of the target gas. The acoustic signal generated in this cell is measured with a commercial electret microphone linked to a lock-in amplifier synchronized to the chopper's frequency.

By testing several concentrations of the target gas in the atmospheric cell and recording the corresponding acoustic signal intensity, a calibration curve can be made. A fitting algorithm based on Beer-Lambert's law approximating a strong saturation of several absorption lines allow producing a reference curve which can then be used to deduce unknown gas concentrations in the atmospheric cell based on the photoacoustic signal, as shown in Fig. 21. To avoid pressure line broadening effect, all measurements are taken at 1 atm. Neutral N_2 gas is used to reach the desired pressure for concentrations of CH_4 below 100%. The small discrepancy between the experimental measurements and the fitted curve that can be seen in Fig. 21 is mostly caused

Optics EXPRESS

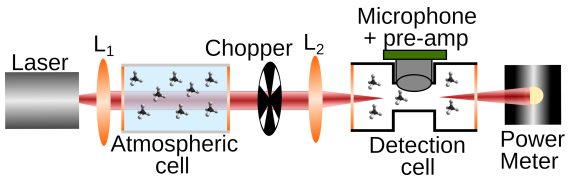

Fig. 20. Experimental setup for photoacoustic methane sensing

by the uncertainty in the CH_4 concentration placed in the atmospheric cell (accuracy error). Aside from reducing the cost of the detection system, this technique has the advantage of a very large dynamic range, and is able to detect even very large concentrations of gas due to the weaker absorption lines of the gas that do not saturate combined with the broad light spectrum. Moreover, simultaneous multi-gas remote sensing can be envisioned with a similar approach where a photoacoustic cell containing a second target gas is added to the system.

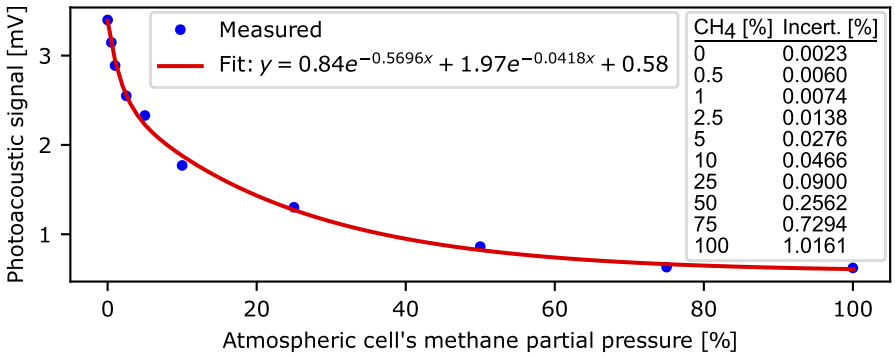

Fig. 21. Preliminary experimental results for photoacoustic methane sensing.

4.2. Polymer processing

The study of polymer processing in the mid-IR has been mostly limited until now by the availability of laser sources. Previous studies of mid-IR resonant processing were conducted by complex sources such as free-electron lasers [171] or OPOs [172]. New alternatives have arisen with the development of fiber sources operating in the 3.3 μm to 3.5 μm band based on the erbium and dysprosium ions. A 3.44 μm fiber laser based on a dual-wavelength pumping scheme has previously been used to study resonant polymer ablation, proving a worthy alternative to current CO_2 laser processing technologies [18]. More recently, the increase in performance of dysprosium-doped fiber lasers has shown such systems to be a promising alternative, their emission reaching wavelengths comparable to the $^4F_{9/2} \rightarrow {}^4I_{11/2}$ that of erbium with a power level up to 3 W [63]. Using an output power of only 134 mW at 3388 nm, preliminary polymer processing results were reported for PMMA [64]. With a power level of a few watts at 3.42 μm coming from a dysprosium-doped fiber laser [63], early studies on the processing of HDPE (high-density polyethylene) and UHMWPE (ultra-high-molecular-weight polyethylene) were conducted, two polymers which lack absorption bands at the wavelengths of the industry-standard CO_2 lasers. These studies were conducted using a setup and methods similar to the ones described by Frayssinous *et al.* [18]. Figure 22 presents the sublimation rates thus obtained with a dysprosium fiber laser at 3.42 μm as a function of fluence, with a CW power of 1.14 W. Given the similar properties of both of these polymers, they exhibit a similar ablation threshold and efficiency. While more studies are required before such laser systems can be used in an industrial

Optics EXPRESS

setting, including comparisons with current systems, these preliminary results show the great potential of resonant polymer ablation with mid-IR fiber lasers.

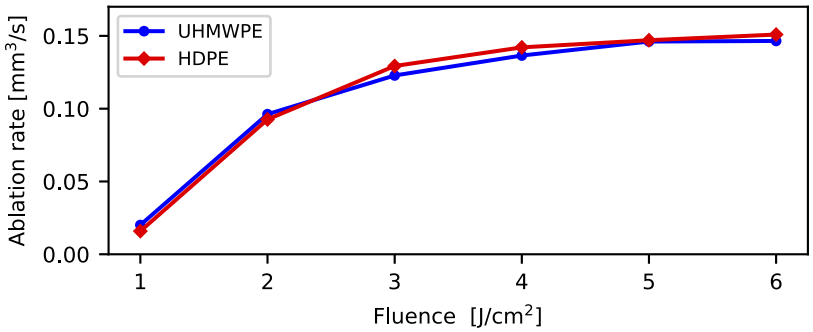

Fig. 22. Ablation rate as a function of fluence for UHMWPE and HDPE with 1.14 W of laser power at 3.42 μm

5. Conclusion

The past few years have seen great progress in the field of mid-IR fiber lasers. With the development and availability of novel fluoride fiber components, laser systems have increased in performance, robustness and diversity, now beginning to see use in a number of applications in the biomedical, environmental, industrial and defense areas. In this paper, we have reviewed notable recent demonstrations of such fiber lasers in both the CW and pulsed regimes and discussed selected applications pertaining to methane sensing and polymer processing.

In CW operation, fiber lasers have seen great improvements, their wavelength coverage [63,64] and output power [53,55,56,68] having drastically increased. Pulsed lasers at 2.8 μm can now achieve hundred microjoules of pulse energy [104,105] while those beyond 3 μm have reached the watt level with energies between 10 μJ-20 μJ [123,125] and new components have enabled erbium-doped lasers near 3 μm to achieve more robust architectures [43]. Such improved architectures have also increased the achievable output power of picosecond pulsed systems near 2.8 μm to the millijoule level [127]. Ultrafast lasers beyond 3 μm have seen their first demonstrations, both for dysprosium [151,152] and erbium at 3.5 μm [153,154]. Ultrafast based sources, for their part, have allowed shifting solitons to wavelengths approaching 5 μm [155].

Although these developments show the great potential of mid-IR fiber lasers, much remains to be achieved. As a matter of fact, the long promised 100 W class 3 μm fiber laser still has to be demonstrated as well as future power scaling towards tens of watts for lasers emitting in the 3.2-3.5 μm spectral region. Pulsed fiber lasers still have significant potential, as sources emitting pulses with energies greater than a hundred microjoules remain to be achieved beyond the 2.8 μm band. Further progress of such sources will also come from an increasingly monolithic architecture, which will become feasible with further developments of fiberized components such as optical isolators suitable for mid-IR operation. Ultrafast fiber lasers will also greatly benefit from the existence of such components, and allow increased wavelength coverage and performances, especially for the dysprosium and erbium laser transitions beyond 3 μm.

The interest in mid-IR fiber lasers is mainly driven by their great potential in a variety of applications. As robust and powerful sources emitting light with varied characteristics become more and more widely available, their use increases in several fields, including in material processing and gas sensing. Although the discussed demonstrations remain preliminary, their promising results are the sign that fiber lasers are only beginning to reach their true potential and that we can hope for great progress in the years to come.

Optics EXPRESS

Funding. Natural Sciences and Engineering Research Council of Canada (CRDPJ-543631-19, CREAT 484907-16, IRCPJ469414-18, RGPIN-2016-05877, RGPIN-2020-04267); Canada First Research Excellence Fund (Sentinel North Program); Canada Foundation for Innovation (5180); Fonds de recherche du Québec – Nature et technologies (114616, CO256655).

Acknowledgments. The authors want to thank S. Albos for her work on methane sensing during her internship. We also thank B. Dussardier and his research group from Université de Nice for the dysprosium-doped silica fiber and fruitful discussions for the Q-switched all-fiber laser project.

Disclosures. The authors declare no conflicts of interest.

Data availability. Data underlying the results presented in this paper are not publicly available at this time but may be obtained from the authors upon reasonable request.

References

1. S. Jackson, M. Bernier, and R. Vallée, eds., *Mid-Infrared Fiber Photonics* (Elsevier, 2021), p. xiii, 1st ed.
2. "International Standard ISO 20473 Optics and Photonics - Spectral bands, (2007)," ISO (2007).
3. M. G. Drexhage and C. T. Moynihan, "Infrared Optical Fibers," Sci. Am. **259**(5), 110–116 (1988).
4. M. Saad, "Fluoride glass fiber: state of the art, in *Fiber Optic Sensors and Applications VI*, vol. 7316 E. Udd, H. H. Du, and A. Wang, eds., International Society for Optics and Photonics (SPIE, 2009), pp. 170–185.
5. T. Klink, G. Schlunck, W. E. Lieb, J. Klink, and F. Grehn, "Long-term results of Erbium YAG-laser-assisted deep sclerectomy," Eye **22**(3), 370–374 (2008).
6. J. D. Holcomb, "Versatility of Erbium YAG Laser: From Fractional Skin Rejuvenation to Full-Field Skin Resurfacing," Facial Plast. Surg. Clin. North Am. **19**(2), 261–273 (2011).
7. J. Diaci and B. Gaspirc, "Comparison of Er:YAG and Er, Cr:YSGG lasers used in dentistry," J. Laser Heal. academy **2012**(6), 1–13 (2012).
8. C.-K. Chen, N.-J. Chang, J.-H. Ke, E. Fu, and W. H. Lan, "Er:YAG laser application for removal of keratosis using topical anesthesia," J. Dental Sci. **8**(2), 196–199 (2013).
9. R. F. Bonner, L. G. Prevosti, M. B. Leon, K. Levin, and D. Tran, "New Source For Laser Angioplasty: Er:YAG Laser Pulses Transmitted Through Zirconium Fluoride Optical Fiber Catheters," in *Optical Fibers in Medicine III*, vol. 0906 A. Katzir, ed., International Society for Optics and Photonics (SPIE, 1988), pp. 288–295.
10. G. M. Hale and M. R. Querry, "Optical Constants of Water in the 200-nm to 200-µm Wavelength Region," Appl. Opt. **12**(3), 555–563 (1973).
11. M. C. Pierce, S. D. Jackson, M. R. Dickinson, T. A. King, and P. Sloan, "Laser-tissue interaction with a continuous wave 3-µm fibre laser: Preliminary studies with soft tissue," Lasers Surg. Med. **26**, 491–495 (2000).
12. M. H. Niemz, *Laser-Tissue Interactions* (Springer International Publishing, 2019), chap. 3.
13. A. Schliesser, N. Picqué, and T. W. Hänsch, "Mid-infrared frequency combs," Nat. Photonics **6**(7), 440–449 (2012).
14. B. M. Walsh, H. R. Lee, and N. P. Barnes, "Mid infrared lasers for remote sensing applications," J. Lumin. **169**, 400–405 (2016).
15. J. Hodgkinson and R. P. Tatam, "Optical gas sensing: A review," Meas. Sci. Technol. **24**(1), 012004 (2013).
16. M. F. S. Ferreira, E. Castro-Camus, D. J. Ottaway, J. M. López-Higuera, X. Feng, W. Jin, Y. Jeong, N. Picqué, L. Tong, B. M. Reinhard, P. M. Pellegrino, A. Méndez, M. Diem, F. Vollmer, and Q. Quan, "Roadmap on optical sensors," J. Opt. (Bristol, U. K.) **19**(8), 083001 (2017).
17. R. Srinivasan and V. Mayne-Banton, "Self-developing photoetching of poly(ethylene terephthalate) films by far-ultraviolet excimer laser radiation," Appl. Phys. Lett. **41**(6), 576–578 (1982).
18. C. Frayssinous, V. Fortin, J. P. Bérubé, A. Fraser, and R. Vallée, "Resonant polymer ablation using a compact 3.44 µm fiber laser," J. Mater. Process. Technol. **252**, 813–820 (2018).
19. S. P. Mahulikar, H. R. Sonawane, and G. Arvind Rao, "Infrared signature studies of aerospace vehicles," Prog. Aerosp. Sci. **43**(8), 218–245 (2007).
20. H. Kaushal, V. Jain, and S. Kar, *Free Space Optical Communication* (Springer India, 2017), vol. 7 of *Optical Networks*, chap. 1.
21. I. Elder, "Performance requirements for countermeasures lasers," in *Technologies for Optical Countermeasures VII*, vol. 7836 D. H. Titterton and M. A. Richardson, eds., International Society for Optics and Photonics (SPIE, 2010), pp. 24–37.
22. E. Luzhansky, F.-S. Choa, S. Merritt, A. Yu, and M. Krainak, "Mid-IR free-space optical communication with quantum cascade lasers," in *Laser Radar Technology and Applications XX; and Atmospheric Propagation XII*, vol. 9465 M. D. Turner, G. W. Kamerman, L. M. W. Thomas, and E. J. Spillar, eds., International Society for Optics and Photonics (SPIE, 2015), pp. 267–273.
23. D. Jung, S. Bank, M. L. Lee, and D. Wasserman, "Next-generation mid-infrared sources," J. Opt. (Bristol, U. K.) **19**(12), 123001 (2017).
24. P. Figueiredo, M. Suttinger, R. Go, E. Tsvid, C. K. N. Patel, and A. A. Lyakh, "Progress in high-power continuous-wave quantum cascade lasers [Invited]," Appl. Opt. **56**(31), H15–H23 (2017).
25. M. Ebrahim-Zadeh and S. Chaitanya Kumar, "Yb-fiber-laser-pumped ultrafast frequency conversion sources from the mid-infrared to the ultraviolet," IEEE J. Select. Topics Quantum Electron. **20**(5), 7600519 (2014).

Optics EXPRESS

26. S. C. Kumar, P. G. Schunemann, K. T. Zawilski, and M. Ebrahim-Zadeh, "Advances in ultrafast optical parametric sources for the mid-infrared based on cdsip2," J. Opt. Soc. Am. B **33**(11), D44–D56 (2016).
27. T. Sanamyan, J. W. Evans, and S. A. McDaniel, "Path to doubling the efficiency of mid-IR erbium lasers," Opt. Express **25**(14), 16452–16457 (2017).
28. S. B. Mirov, I. S. Moskalev, S. Vasilyev, V. Smolski, V. V. Fedorov, D. Martyshkin, J. Peppers, M. Mirov, A. Dergachev, and V. Gapontsev, "Frontiers of mid-ir lasers based on transition metal doped chalcogenides," IEEE J. Select. Topics Quantum Electron **24**(5), 1–29 (2018).
29. M. R. Majewski, R. I. Woodward, J.-Y. Carrée, S. Poulain, M. Poulain, and S. D. Jackson, "Emission beyond 4 μm and mid-infrared lasing in a dysprosium-doped indium fluoride (InF_3) fiber," Opt. Lett. **43**(8), 1926–1929 (2018).
30. B. Wang, L. Cheng, H. Zhong, J. Sun, Y. Tian, X. Zhang, and B. Chen, "Excited state absorption cross sections of $^4I_{13/2}$ of Er^{3+} in ZBLAN," Opt. Mater. (Amsterdam, Neth.) **31**(11), 1658–1662 (2009).
31. J. Li, L. Gomes, and S. D. Jackson, "Numerical Modeling of Holmium-Doped FLuoride Fiber Lasers," IEEE J. Quantum Electron. **48**(5), 596–606 (2012).
32. O. Henderson-Sapir, A. Malouf, N. Bawden, J. Munch, S. D. Jackson, and D. J. Ottaway, "Recent advances in 3.5 μm Erbium-Doped Mid-Infrared Fiber Lasers," IEEE J. Select. Topics Quantum Electron. **23**(3), 6–14 (2016).
33. C. Carbonnier, H. Többen, and U. Unrau, "Room temperature CW fibre laser at 3.22 μm," Electron. Lett. **34**(9), 893–894 (1998).
34. M. R. Majewski and S. D. Jackson, "Highly efficient mid-infrared dysprosium fiber laser," Opt. Lett. **41**(10), 2173–2176 (2016).
35. O. Henderson-sapir, "Development of dual-wavelength pumped mid-infrared fibre laser," Ph.D. thesis, University of Adelaide (2015).
36. L. Gomes, V. Fortin, M. Bernier, R. Vallée, S. Poulain, M. Poulain, and S. D. Jackson, "The basic spectroscopic parameters of Ho^{3+}-doped fluoroindate glass for emission at 3.9 μm," Opt. Mater. (Amsterdam, Neth.) **60**, 618–626 (2016).
37. T. Taunay, H. Poignant, S. Boj, P. Niay, P. Bernage, E. Delevaque, M. Monerie, and E. X. Xie, "Ultraviolet-induced permanent Bragg gratings in cerium-doped ZBLAN glasses or optical fibers," Opt. Lett. **19**(17), 1269–1271 (1994).
38. M. Bernier, D. Faucher, R. Vallée, A. Saliminia, G. Androz, Y. Sheng, and S. L. Chin, "Bragg gratings photoinduced in ZBLAN fibers by femtosecond pulses at 800 nm," Opt. Lett. **32**(5), 454–456 (2007).
39. N. Caron, M. Bernier, D. Faucher, and R. Vallée, "Understanding the fiber tip thermal runaway present in 3 μm fluoride glass fiber lasers," Opt. Express **20**(20), 22188–22194 (2012).
40. F. Maes, V. Fortin, M. Bernier, and R. Vallée, "5.6 W monolithic fiber laser at 3.55 μm," Opt. Lett. **42**(11), 2054–2057 (2017).
41. C. A. Schäfer, H. Uehara, D. Konishi, S. Hattori, H. Matsukuma, M. Murakami, S. Shimizu, and S. Tokita, "Fluoride-fiber-based side-pump coupler for high-power fiber lasers at 2.8 μm," Opt. Lett. **43**(10), 2340–2343 (2018).
42. S. Magnan-Saucier, S. Duval, C. Matte-Breton, Y. O. Aydin, V. Fortin, S. LaRochelle, M. Bernier, and R. Vallée, "Fuseless side-pump combiner for efficient fluoride-based double-clad fiber pumping," Opt. Lett. **45**(20), 5828–5831 (2020).
43. P. Paradis, V. Fortin, S. Trzesien, M. Ude, B. Dussardier, R. Vallée, and M. Bernier, "Dysprosium-Doped Silica Fiber as Saturable Absorber in a Mid-IR Fiber Laser," in *2021 IEEE Photonics Conference (IPC)*, (IEEE, 2021), p. WH3.2.
44. Y. O. Aydin, F. Maes, V. Fortin, S. Toubou Bah, R. Vallée, and M. Bernier, "Endcapping of high-power 3 μm all-fiber lasers," Opt. Express **27**(15), 20659–20669 (2019).
45. V. Fortin, M. Bernier, S. T. Bah, and R. Vallée, "30 W fluoride glass all-fiber laser at 2.94 μm," Opt. Lett. **40**(12), 2882–2885 (2015).
46. M. Poulain, M. Poulain, and J. Lucas, "Verres fluores au tetrafluorure de zirconium proprietes optiques d'un verre dope au Nd^{3+}," Mater. Res. Bull. **10**(4), 243–246 (1975).
47. M. Brierley and P. France, "Continuous wave lasing at 2.7 μm in an erbium-doped fluorozirconate fibre," Electron. Lett. **24**(15), 935–936 (1988).
48. L. Wetenkamp, "Efficient CW operation of a 2.9 μm Ho^{3+}-doped fluorozirconate fibre laser pumped at 640 nm," Electron. Lett. **26**(13), 883–884 (1990).
49. H. Többen, "Cw lasing at 3.45 μm in erbium-doped fluorozirconate fibres," Frequenz **45**(10), 250–252 (1991).
50. H. Többen, "Room temperature cw fiber laser at 3.5 μm in Er^{3+}-doped ZBLAN glass," Electron. Lett. **28**(14), 2–3 (1992).
51. J. Schneide, C. Carbonnier, and U. B. Unrau, "Characterization of a Ho^{3+}-doped fluoride fiber laser with a 3.9-μm emission wavelength," Appl. Opt. **36**(33), 8595–8600 (1997).
52. S. D. Jackson, "Continuous wave 2.9 μm dysprosium-doped fluoride fiber laser," Appl. Phys. Lett. **83**(7), 1316–1318 (2003).
53. Y. O. Aydin, V. Fortin, R. Vallée, and M. Bernier, "Towards power scaling of 2.8 μm fiber lasers," Opt. Lett. **43**(18), 4542–4545 (2018).
54. S. Crawford, D. D. Hudson, and S. D. Jackson, "High-Power Broadly Tunable 3-μm Fiber Laser for the Measurement of Optical Fiber Loss," IEEE Photonics J. **7**(3), 1–9 (2015).

Optics EXPRESS

55. V. Fortin, F. Jobin, M. Larose, M. Bernier, and R. Vallée, "10-W-level monolithic dysprosium-doped fiber laser at 3.24 µm," Opt. Lett. **44**(3), 491–494 (2019).
56. M. Lemieux-Tanguay, V. Fortin, T. Boilard, P. Paradis, F. Maes, L. Talbot, R. Vallée, and M. Bernier, "15 W Monolithic FIber Laser at 3.55 µm," Opt. Lett. **47**(2), 289–292 (2021).
57. W. Shi, Q. Fang, X. Zhu, R. A. Norwood, and N. Peyghambarian, "Fiber lasers and their applications [Invited]," Appl. Opt. **53**(28), 6554–6568 (2014).
58. O. Henderson-sapir, J. Munch, and D. J. Ottaway, "A Higher Power 3.5 µm Fibre Laser," Advanced Solid-State Lasers pp. 5–7 (2014).
59. Y. O. Aydin, V. Fortin, F. Maes, F. Jobin, S. D. Jackson, R. Vallée, and M. Bernier, "Diode-pumped mid-infrared fiber laser with 50% slope efficiency," Optica **4**(2), 6–9 (2017).
60. S. D. Jackson, "High-power and highly efficient diode-cladding-pumped holmium-doped fluoride fiber laser operating at 2.94 µm," Opt. Lett. **34**(15), 2327–2329 (2009).
61. L. Sojka, L. Pajewski, M. Popenda, E. Beres-Pawlik, S. Lamrini, K. Markowski, T. Osuch, T. M. Benson, A. B. Seddon, and S. Sujecki, "Experimental Investigation of Mid-Infrared Laser Action From Dy^{3+}-Doped Fluorozirconate Fiber," IEEE Photon. Technol. Lett. **30**(12), 1083–1086 (2018).
62. R. I. Woodward, M. R. Majewski, G. Bharathan, D. D. Hudson, A. Fuerbach, and S. D. Jackson, "Watt-level dysprosium fiber laser at 3.15 µm with 73% slope efficiency," Opt. Lett. **43**(7), 1471–1474 (2018).
63. L.-P. Pleau, V. Fortin, T. Boilard, F. Jobin, R. Vallee, Y. Messaddeq, and M. Bernier, "Long wavelength multi-watt dysprosium fiber laser for resonant polymer ablation," in *Laser Congress 2021 (ASSL, LAC)*, (Optical Society of America, 2021), p. ATu4A.7.
64. M. R. Majewski, G. Bharathan, A. Fuerbach, and S. D. Jackson, "Long wavelength operation of a dysprosium fiber laser for polymer processing," Opt. Lett. **46**(3), 600–603 (2021).
65. F. Maes, C. Stihler, L.-P. Pleau, V. Fortin, J. Limpert, M. Bernier, and R. Vallée, "3.42 µm lasing in heavily-erbium-doped fluoride fibers," Opt. Express **27**(3), 2170–2183 (2019).
66. O. Henderson-Sapir, S. D. Jackson, and D. J. Ottaway, "Versatile and widely tunable mid-infrared erbium doped ZBLAN fiber laser," Opt. Lett. **41**(7), 1676–1679 (2016).
67. Z. Qin, G. Xie, J. Ma, P. Yuan, and L. Qian, "Mid-infrared Er:ZBLAN fiber laser reaching 3.68 µm wavelength," Chin. Opt. Lett. **15**, 111402 (2017).
68. F. Maes, V. Fortin, S. Poulain, M. Poulain, J.-Y. Carrée, M. Bernier, and R. Vallée, "Room-temperature fiber laser at 3.92 µm," Optica **5**(7), 761–764 (2018).
69. S. D. Jackson and R. Jain, "Fiber-Based Sources of Coherent Mid-infrared Radiation: Key Advances and Future Prospects," Opt. Express **28**(21), 30964–31019 (2020).
70. R. Vallée, M. Bernier, and D. Faucher, "System and Method for Permanently Writing a Diffraction Grating in a Low Phonon Energy Glass Medium," U.S. patent 8,078,023 (13 December 2011).
71. J. Habel, T. Boilard, J.-S. Frenière, F. Trépanier, and M. Bernier, "Femtosecond FBG Written through the Coating for Sensing Applications," Sensors **17**(11), 2519 (2017).
72. M. Bernier, R. Vallée, F. Trépanier, and J. Carrier, "Writing of high mechanical strength fiber bragg gratings using ultrafast pulses and a phase mask," U.S. patent 10,845,533 (24 November 2020).
73. M. R. Majewski, M. Z. Amin, T. Berthelot, and S. D. Jackson, "Directly diode-pumped mid-infrared dysprosium fiber laser," Opt. Lett. **44**(22), 5549–5552 (2019).
74. J. Wang, X. Zhu, R. A. Norwood, and N. Peyghambarian, "Beyond 3 µm Dy^{3+}/Er^{3+} co-doped ZBLAN fiber lasers pumped by 976 nm laser diode," Appl. Phys. Lett. **118**(15), 151101 (2021).
75. L.-C. Michaud, T. Boilard, V. Fortin, S. Magnan-Saucier, R. Vallée, and M. Bernier, "Thermally tunable all-fiber laser operating at 3.24 µm for remote sensing of methane," in *Laser Congress 2021 (ASSL, LAC)*, (Optical Society of America, 2021), p. AM4A.3.
76. M. R. Majewski, R. I. Woodward, S. D. Jackson, and N. Ryde, "Dysprosium-doped ZBLAN fiber laser tunable from 2.8 µm to 3.4 µm, pumped at 1.7 µm," Opt. Lett. **43**(5), 971–974 (2018).
77. O. Henderson-Sapir, J. Munch, and D. J. Ottaway, "Mid-infrared fiber lasers at and beyond 3.5 µm using dual-wavelength pumping," Opt. Lett. **39**(3), 493–496 (2014).
78. V. Fortin, F. Maes, M. Bernier, S. T. Bah, M. D'Auteuil, and R. Vallée, "Watt-level erbium-doped all-fiber laser at 3.44 µm," Opt. Lett. **41**(3), 559–562 (2016).
79. S. Cozic, S. Boivinet, C. Pierre, J. Boulet, S. Poulain, and M. Poulain, "Splicing fluoride glass and silica optical fibers," in *EPJ Web of Conferences*, vol. 215 O. Fähnle and A. Vasdekis, eds. (2019), p. 04003.
80. F. Maes, V. Fortin, M. Bernier, and R. Vallee, "Quenching of 3.4 µm Dual-Wavelength Pumped Erbium Doped Fiber Lasers," IEEE J. Quantum Electron. **53**(2), 1–8 (2017).
81. L. Gomes, V. Fortin, M. Bernier, F. Maes, R. Vallée, S. Poulain, M. Poulain, and S. D. Jackson, "Excited state absorption and energy transfer in Ho^{3+}-doped indium fluoride glass," Opt. Mater. (Amsterdam, Neth.) **66**, 519–526 (2017).
82. H. Uehara, D. Konishi, K. Goya, R. Sahara, M. Murakami, and S. Tokita, "Power scalable 30-W mid-infrared fluoride fiber amplifier," Opt. Lett. **44**(19), 4777–4780 (2019).
83. M. Z. Amin, M. R. Majewski, R. I. Woodward, A. Fuerbach, and S. D. Jackson, "Novel Near-infrared Pump Wavelengths for Dysprosium Fiber Lasers," J. Lightwave Technol. **38**(20), 5801–5808 (2020).

Optics EXPRESS

84. S. D. Jackson and A. Lauto, "Diode-pumped fiber lasers: A new clinical tool?" Lasers Surg. Med. **30**, 184–190 (2002).
85. W. M. Steen, "Laser material processing-an overview," J. Opt. A: Pure Appl. Opt. **5**(4), S3–S7 (2003).
86. W. M. Steen and J. Mazumder, *Laser material processing* (Springer science & business media, 2010), chap. 3, 4.
87. J. Mandon, G. Guelachvili, and N. Picqué, "Fourier transform spectroscopy with a laser frequency comb," Nat. Photonics **3**(2), 99–102 (2009).
88. T. Udem, "Spectroscopy: Frequency comb benefits," Nat. Photonics **3**(2), 82–84 (2009).
89. M. Vainio and L. Halonen, "Mid-infrared optical parametric oscillators and frequency combs for molecular spectroscopy," Phys. Chem. Chem. Phys. **18**(6), 4266–4294 (2016).
90. C. Matte-Breton, S. Larochelle, S. Duval, R. Vallée, and M. Bernier, "Method of coupling optical fibers, and optical coupler," WIPO|PCT patent WO2021030911A1 (5 February 2021).
91. Q. Xiao, P. Yan, S. Y. Hao, and M. Gong, "100 W ytterbium-doped monolithic fiber laser with fused angle-polished side-pumping configuration," Laser Phys. Lett. **129**(2), 125–129 (2011).
92. Q. Xiao, P. Yan, Y. Wang, J. Hao, X. Zhang, and M. Gong, "Fused angle-polished multi-points side-pumping coupler for monolithic fiber lasers and amplifiers," Opt. Commun. **285**(8), 2137–2143 (2012).
93. Å. Rosenqvist, A. Milne, R. Lucas, M. Imhoff, and C. Dobson, "A review of remote sensing technology in support of the Kyoto Protocol," Environ. Sci. Policy **6**(5), 441–455 (2003).
94. F. K. Tittel, D. Richter, and A. Fried, "Mid-infrared laser applications in spectroscopy," *Solid-State Mid-Infrared Laser Sources* 516, 445–516 (Springer, 2003).
95. D. Bäuerle, "Laser processing and chemistry: recent developments," Appl. Surf. Sci. **186**(4), 1–6 (2002).
96. S. M. O'Malley, J. Schoeffling, R. Jimenez, B. Zinderman, S. Y. Yi, and D. M. Bubb, "The influence of wavelength, temporal sequencing, and pulse duration on resonant infrared matrix-assisted laser processing of polymer films," Appl. Phys. A: Mater. Sci. Process. **117**(3), 1343–1351 (2014).
97. P. Paradis, V. Fortin, Y. O. Aydin, R. Vallée, and M. Bernier, "10 W-level gain-switched all-fiber laser at 2.8 μm," Opt. Lett. **43**(13), 3196–3199 (2018).
98. A. S. Kurkov, "Q-switched all-fiber lasers with saturable absorbers," Laser Phys. Lett. **8**, 335–342 (2011).
99. L. Tordella, H. Djellout, B. Dussardier, A. Saïssy, and G. Monnom, "High repetition rate passively Q-switched Nd^{3+}:Cr^{4+} all-fibre laser," Electron. Lett. **39**(18), 1307–1308 (2003).
100. B. Dussardier, J. Maria, and P. Peterka, "Passively Q-switched ytterbium- and chromium-doped all-fiber laser," Appl. Opt. **50**(25), E20–E23 (2011).
101. S. D. Jackson, "Passively Q-switched Tm^{3+}-doped silica fiber lasers," Appl. Opt. **46**(16), 3311–3317 (2007).
102. A. Kurkov, E. Sholokhov, and O. Medvedkov, "All fiber Yb-Ho pulsed laser," Laser Phys. Lett. **6**, 135–138 (2008).
103. S. Tokita, M. Murakami, S. Shimizu, M. Hashida, and S. Sakabe, "12 W Q-switched Er:ZBLAN fiber laser at 2.8 μm," Opt. Lett. **36**(15), 2812–2814 (2011).
104. S. Lamrini, K. Scholle, M. Schäfer, J. Ward, M. Francis, M. Farries, S. Sujecki, T. Benson, A. Seddon, A. Oladeji, B. Napier, and P. Fuhrberg, "High-Energy Q-switched Er:ZBLAN Fibre Laser at 2.79 μm," in *2015 European Conference on Lasers and Electro-Optics - European Quantum Electronics Conference*, (Optical Society of America, 2015), p. CJ_7_2.
105. L. Sójka, L. Pajewski, S. Lamrini, M. Farries, T. M. Benson, B. Angela, L. Sojka, L. Pajewski, S. Lamrini, M. Farries, T. M. Benson, A. B. Seddon, and S. Sujecki, "High peak power Q-switched Er:ZBLAN fiber laser," J. Lightwave Technol. **8724**(20), 6572–6578 (2021).
106. Z. Qin, G. Xie, J. Ma, P. Yuan, and L. Qian, "2.8 μm all-fiber Q-switched and mode-locked lasers with black phosphorus," Photon. Res. **6**(11), 1074–1078 (2018).
107. J. Wang, J. Wei, W. Liu, P. Yan, C. Guo, C. Ye, L. Xia, and S. Ruan, "2.8 μm passively Q-switched Er:ZBLAN fiber laser with an Sb saturable absorber mirror," Appl. Opt. **59**(29), 9165–9168 (2020).
108. S. Wang, Y. Tang, J. Yang, H. Zhong, and D. Fan, "MoS_2 Q -switched 2.8 μm Er:ZBLAN fiber laser," Laser Phys. **29**(2), 025101 (2019).
109. Y. Shen, Y. Wang, K. Luan, K. Huang, M. Tao, H. Chen, A. Yi, G. Feng, and J. Si, "Watt-level passively Q-switched heavily Er^{3+}-doped ZBLAN fiber laser with a semiconductor saturable absorber mirror," Sci. Rep. **6**(1), 26659 (2016).
110. C. Wei, X. Zhu, R. A. Norwood, and N. Peyghambarian, "Passively Q-Switched 2.8-μm Nanosecond Fiber Laser," IEEE Photon. Technol. Lett. **24**(19), 1741–1744 (2012).
111. Y. Shen, Y. Wang, F. Zhu, L. Ma, L. Zhao, Z. Chen, H. Wang, C. Huang, K. Huang, and G. Feng, "200 μJ, 13 ns Er:ZBLAN mid-infrared fiber laser actively Q-switched by an electro-optic modulator," Opt. Lett. **46**(5), 1141–1144 (2021).
112. Y. Wang and H. Luo, "Wavelength-tunable, linearly polarized Q-switched and gain-switched polarization-maintaining Er^{3+}-doped fluoride fiber laser in the range of 2.7~2.83 μm," Opt. Commun. **504**, 127482 (2022).
113. R. I. Woodward, M. R. Majewski, N. Macadam, G. Hu, T. Albrow-Owen, T. Hasan, and S. D. Jackson, "Q-switched Dy:ZBLAN fiber lasers beyond 3 μm: comparison of pulse generation using acousto-optic modulation and inkjet-printed black phosphorus," Opt. Express **27**(10), 15032–15045 (2019).
114. H. Luo, J. Li, Y. Gao, Y. Xu, X. Li, and Y. Liu, "Tunable passively Q-switched Dy^{3+}-doped fiber laser from 2.71 to 3.08 μm using PbS nanoparticles," Opt. Lett. **44**(9), 2322–2325 (2019).

Optics EXPRESS

115. N. Bawden, H. Matsukuma, O. Henderson-Sapir, E. Klantsataya, S. Tokita, and D. J. Ottaway, "Actively Q-switched dual-wavelength pumped Er^{3+}:ZBLAN fiber laser at 3.47 μm," Opt. Lett. **43**(11), 2724–2727 (2018).
116. J. Liu, J. Wu, P. Tang, Y. Chen, and D. Fan, "3.5 μm self-Q-switched Er^{3+}:ZBLAN fiber laser stabilized by an ASE seeded pump source," in *Conference on Lasers and Electro-Optics*, (Optical Society of America, 2019), p. SF2L.2.
117. Z. Fang, C. Zhang, J. Liu, Y. Chen, and D. Fan, "3.46 μm Q-switched Er^{3+}:ZBLAN fiber laser based on a semiconductor saturable absorber mirror," Opt. Laser Technol. **141**, 107131 (2021).
118. H. Luo, J. Yang, J. Li, and Y. Liu, "Widely tunable passively Q-switched Er^{3+}-doped ZrF_4 fiber laser in the range of 3.4-3.7 μm based on a Fe^{2+}:ZnSe crystal," Photon. Res. **7**(9), 1106–1111 (2019).
119. Z. Qin, T. Hai, G. Xie, J. Ma, P. Yuan, L. Qian, L. Li, L. Zhao, and D. Shen, "Black phosphorus Q-switched and mode-locked mid-infrared Er:ZBLAN fiber laser at 3.5 μm wavelength," Opt. Express **26**(7), 8224–8231 (2018).
120. M. Gorjan, R. Petkovšek, M. Marinček, and M. Čopič, "High-power pulsed diode-pumped Er:ZBLAN fiber laser," Opt. Lett. **36**(10), 1923–1925 (2011).
121. H. Luo, Y. Xu, J. Li, and Y. Liu, "Gain-switched dysprosium fiber laser tunable from 2.8 to 3.1 μm," Opt. Express **27**(19), 27151–27158 (2019).
122. L. Pajewski, L. Sójka, S. Lamrini, T. M. Benson, A. B. Seddon, and S. Sujecki, "Gain-switched Dy^{3+}:ZBLAN fiber laser operating around 3 μm," J. Physics: Photonics **2**, 014003 (2019).
123. F. Jobin, P. Paradis, V. Fortin, S. Magnan-Saucier, M. Bernier, and R. Vallee, "1.4 W in-band pumped Dy^{3+}-doped gain-switched fiber laser at 3.24 μm," Opt. Lett. **45**(18), 5028–5031 (2020).
124. F. Jobin, V. Fortin, F. Maes, M. Bernier, and R. Vallée, "Gain-switched fiber laser at 3.55 μm," Opt. Lett. **43**(8), 1770–1773 (2018).
125. H. Luo, J. Yang, F. Liu, Z. Hu, Y. Xu, F. Yan, H. Peng, F. Ouellette, J. Li, and Y. Liu, "Watt-level gain-switched fiber laser at 3.46 μm," Opt. Express **27**(2), 1367–1375 (2019).
126. J. Yang, H. Luo, F. Liu, J. Li, and Y. Liu, "Widely tunable gain-switched Er^{3+}-doped ZrF_4 fiber laser from 3.4 to 3.7 μm," IEEE Photon. Technol. Lett. **32**(20), 1335–1338 (2020).
127. Y. O. Aydin, S. Magnan-Saucier, D. Zhang, V. Fortin, D. Kraemer, R. Vallée, and M. Bernier, "Dual stage fiber amplifier operating near 3 μm with millijoule-level, sub-ns pulses at 5 W," Opt. Lett. **46**(18), 4506–4509 (2021).
128. W. Du, X. Xiao, Y. Cui, J. Nees, I. Jovanovic, and A. Galvanauskas, "Demonstration of 0.67-mJ and 10-ns high-energy pulses at 2.72 μm from large core Er:ZBLAN fiber amplifiers," Opt. Lett. **45**(19), 5538–5541 (2020).
129. P. Wan, L.-M. Yang, S. Bai, and J. Liu, "High energy 3 μm ultrafast pulsed fiber laser," Opt. Express **23**(7), 9527–9532 (2015).
130. S. Amini-Nik, D. Kraemer, M. L. Cowan, K. Gunaratne, P. Nadesan, B. A. Alman, and R. J. D. Miller, "Ultrafast Mid-IR Laser Scalpel: Protein Signals of the Fundamental Limits to Minimally Invasive Surgery," PLoS One **5**(9), e13053 (2010).
131. K. Werner, M. G. Hastings, A. Schweinsberg, B. L. Wilmer, D. Austin, C. M. Wolfe, M. Kolesik, T. R. Ensley, L. Vanderhoef, A. Valenzuela, and E. Chowdhury, "Ultrafast mid-infrared high harmonic and supercontinuum generation with n_2 characterization in zinc selenide," Opt. Express **27**(3), 2867–2885 (2019).
132. S. Duval, M. Bernier, V. Fortin, J. Genest, M. Piche, and R. Vallée, "Femtosecond fiber lasers reach the mid-infrared," Optica **2**(7), 623–626 (2015).
133. T. Hu, S. D. Jackson, and D. D. Hudson, "Femtosecond mode-locked pulses from a mid-infrared fiber laser," in *2015 European Conference on Lasers and Electro-Optics - European Quantum Electronics Conference*, (Optica Publishing Group, 2015), p. CJ_5_2.
134. S. Duval, M. Olivier, V. Fortin, M. Bernier, M. Piché, and R. Vallée, "23-kW peak power femtosecond pulses from a mode-locked fiber ring laser at 2.8 μm," Proc. SPIE **9728**, 972802 (2016).
135. S. Antipov, D. D. Hudson, A. Fuerbach, and S. D. Jackson, "High-power mid-infrared femtosecond fiber laser in the water vapor transmission window," Optica **3**(12), 1373–1376 (2016).
136. S. Duval, J.-C. Gauthier, L.-R. Robichaud, P. Paradis, M. Olivier, V. Fortin, M. Bernier, M. Piché, and R. Vallée, "Watt-level fiber-based femtosecond laser source tunable from 2.8 to 3.6 μm," Opt. Lett. **41**(22), 5294–5297 (2016).
137. J. Huang, M. Pang, X. Jiang, F. Köttig, D. Schade, W. He, M. Butryn, and P. S. J. Russell, "Sub-two-cycle octave-spanning mid-infrared fiber laser," Optica **7**(6), 574–579 (2020).
138. Y. Zhou, Z. Qin, P. Yuan, J. Ma, and G. Xie, "2-MW peak-power pulses from a dispersion-managed fluoride fiber amplifier at 2.8 μm," Opt. Lett. **46**(20), 5104–5107 (2021).
139. P. Tang, Z. Qin, J. Liu, C. Zhao, G. Xie, S. Wen, and L. Qian, "Watt-level passively mode-locked Er^{3+}-doped ZBLAN fiber laser at 2.8 μm," Opt. Lett. **40**(21), 4855–4858 (2015).
140. P. Paradis, S. Duval, V. Fortin, R. Vallée, and M. Bernier, "Towards Ultrafast All-Fiber Laser at 2.8 μm Based on a SESAM and a Fiber Bragg Grating," in *The European Conference on Lasers and Electro-Optics*, (Optical Society of America, 2019), p. cf_p_43.
141. G. Bharathan, L. Xu, X. Jiang, H. Zhang, Z. Li, F. Chen, and A. Fuerbach, "MXene and $PtSe_2$ saturable absorbers for all-fibre ultrafast mid-infrared lasers," Opt. Mater. Express **11**(7), 1898–1906 (2021).
142. C. Wei, X. Zhu, R. A. Norwood, and N. Peyghambarian, "Passively continuous-wave mode-locked Er^{3+}-doped ZBLAN fiber laser at 2.8 μm," Opt. Lett. **37**(18), 3849–3851 (2012).
143. Z. Qin, G. Xie, C. Zhao, S. Wen, P. Yuan, and L. Qian, "Mid-infrared mode-locked pulse generation with multilayer black phosphorus as saturable absorber," Opt. Lett. **41**(1), 56–59 (2016).

Optics EXPRESS

144. G. Zhu, X. Zhu, F. Wang, S. Xu, Y. Li, X. Guo, K. Balakrishnan, R. A. Norwood, and N. Peyghambarian, "Graphene mode-locked fiber laser at 2.8 μm," IEEE Photon. Technol. Lett. **28**(1), 7–10 (2015).
145. H. Luo, Y. Wang, J. Li, and Y. Liu, "High-stability, linearly polarized mode-locking generation from a polarization-maintaining fiber oscillator around 2.8 μm," Opt. Lett. **46**(18), 4550–4553 (2021).
146. H. Luo, J. Yang, J. Li, and Y. Liu, "Tunable sub-300 fs soliton and switchable dual-wavelength pulse generation from a mode-locked fiber oscillator around 28 μm," Opt. Lett. **46**(4), 841–844 (2021).
147. J. Li, D. D. Hudson, Y. Liu, and S. D. Jackson, "Efficient 2.87 μm fiber laser passively switched using a semiconductor saturable absorber mirror," Opt. Lett. **37**(18), 3747–3749 (2012).
148. T. Hu, D. D. Hudson, and S. D. Jackson, "Stable, self-starting, passively mode-locked fiber ring laser of the 3 μm class," Opt. Lett. **39**(7), 2133–2136 (2014).
149. K. Yin, T. Jiang, X. Zheng, H. Yu, X. Cheng, and J. Hou, "Mid-infrared ultra-short mode-locked fiber laser utilizing topological insulator Bi_2Te_3 nano-sheets as the saturable absorber," arXiv preprint arXiv:1505.06322 (2015).
150. H. Luo, S. Li, X. Wu, Z. Kang, J. Li, G. Qin, W. Qin, and Y. Liu, "Unlocking the ultrafast potential of gold nanowires for mode-locking in the mid-infrared region," Opt. Lett. **46**(7), 1562–1565 (2021).
151. R. I. Woodward, M. R. Majewski, and S. D. Jackson, "Mode-locked dysprosium fiber laser: Picosecond pulse generation from 2.97 to 3.30 μm," APL Photonics **3**(11), 116106 (2018).
152. Y. Wang, F. Jobin, S. Duval, V. Fortin, P. Laporta, M. Bernier, G. Galzerano, and R. Vallée, "Ultrafast Dy^{3+}:fluoride fiber laser beyond 3 μm," Opt. Lett. **44**(2), 395–398 (2019).
153. O. Henderson-Sapir, N. Bawden, M. R. Majewski, R. I. Woodward, D. J. Ottaway, and S. D. Jackson, "Mode-locked and tunable fiber laser at the 3.5 μm band using frequency-shifted feedback," Opt. Lett. **45**(1), 224–227 (2020).
154. N. Bawden, O. Henderson-Sapir, S. D. Jackson, and D. J. Ottaway, "Ultrafast 3.5 μm fiber laser," Opt. Lett. **46**(7), 1636–1639 (2021).
155. J.-C. Gauthier, P. Paradis, M. Olivier, M.-F. Dumas, R. Vallée, and M. Bernier, "Soliton self-frequency shift up to 4.6 μm in an InF_3 fiber," in *Advanced Solid State Lasers*, (Optical Society of America, 2021), p. ATu4A.5.
156. T. Boilard, R. Vallée, and M. Bernier, "Probing the dispersive properties of optical fibers with an array of femtosecond-written fiber Bragg gratings," arXiv preprint arXiv:2109.13366 (2021).
157. A. Haboucha, V. Fortin, M. Bernier, J. Genest, Y. Messaddeq, and R. Vallée, "Fiber Bragg grating stabilization of a passively mode-locked 2.8 μm Er^{3+}:fluoride glass fiber laser," Opt. Lett. **39**(11), 3294–3297 (2014).
158. M. R. Majewski, M. Pawliszewska, and S. D. Jackson, "Picosecond pulse formation in the presence of atmospheric absorption," Opt. Express **29**(12), 19159–19169 (2021).
159. C. Cutler, "Why does linear phase shift cause mode locking?" IEEE J. Quantum Electron. **28**(1), 282–288 (1992).
160. H. A. Haus, "Mode-Locking of Lasers," IEEE J. Sel. Top. Quantum Electron. **6**(6), 1173–1185 (2000).
161. S. Solomon, "Intergovernmental Panel on Climate Change., and Intergovernmental Panel on Climate Change. Working Group I," *Climate change 2007 : the physical science basis : contribution of Working Group I to the Fourth Assessment Report of the Intergovernmental Panel on Climate Change* (Cambridge University Press, 2007).
162. L. Yu, H. Wang, G. Wang, W. Song, Y. Huang, S.-G. Li, N. Liang, Y. Tang, and J.-S. He, "A comparison of methane emission measurements using eddy covariance and manual and automated chamber-based techniques in Tibetan Plateau alpine wetland," Environ. Pollut. (Oxford, U. K.) **181**, 81–90 (2013).
163. M. K. Pihlatie, J. R. Christiansen, H. Aaltonen, J. F. Korhonen, A. Nordbo, T. Rasilo, G. Benanti, M. Giebels, M. Helmy, J. Sheehy, S. Jones, R. Juszczak, R. Klefoth, R. Lobo-do Vale, A. P. Rosa, P. Schreiber, D. Serça, S. Vicca, B. Wolf, and J. Pumpanen, "Comparison of static chambers to measure CH_4 emissions from soils," Agric. For. Meteorol. **171-172**, 124–136 (2013).
164. M. Gålfalk, G. Olofsson, P. Crill, and D. Bastviken, "Making methane visible," Nat. Clim. Chang. **6**(4), 426–430 (2016).
165. T. Strahl, J. Herbst, A. Lambrecht, E. Maier, J. Steinebrunner, and J. Wöllenstein, "Methane leak detection by tunable laser spectroscopy and mid-infrared imaging," Appl. Opt. **60**(15), C68–C75 (2021).
166. M. Ghysels, L. Gomes, J. Cousin, N. Amarouche, H. Jost, and G. Durry, "Spectroscopy of CH_4 with a difference-frequency generation laser at 3.3 micron for atmospheric applications," Appl. Phys. B **104**(4), 989–1000 (2011).
167. J. Li, Z. Yu, Z. Du, Y. Ji, and C. Liu, "Standoff Chemical Detection Using Laser Absorption Spectroscopy: A Review," Remote. Sens. **12**(17), 2771 (2020).
168. L.-P. Pleau, V. Fortin, F. Maes, R. Vallée, and M. Bernier, "Tunable all-fiber laser for remote sensing of methane near 3.4 μm," in *2019 Conference on Lasers and Electro-Optics Europe and European Quantum Electronics Conference*, (Optica Publishing Group, 2019), p. cj_5_2.
169. M. R. Majewski and S. D. Jackson, "Tunable dysprosium laser," Opt. Lett. **41**(19), 4496–4498 (2016).
170. R. I. Woodward, M. R. Majewski, D. D. Hudson, and S. D. Jackson, "Swept-wavelength mid-infrared fiber laser for real-time ammonia gas sensing," APL Photonics **4**(2), 020801 (2019).
171. D. M. Bubb, J. Horwitz, and M. Papantonakis, "Resonnant Infrared Pulsed Laser Deposition of Polymers Using a Picosecod Tunable Free-Electron Laser," in *Cleo 2002*, vol. 33 (2002), pp. 2–3.
172. S. Naithani, A. Grisard, D. Schaubroeck, E. Lallier, and S. Geert Van, "Mid-Infrared Resonant Ablation of PMMA," J. Laser Micro/Nanoeng. **9**(2), 147–152 (2014).